Check for updates

New Phytologist

Research

Comprehensive genetic analyses of *Arabidopsis* autophagy-related 8 family reveal redundant regulatory roles during autophagy

Kuntian Dong[1]*, Guiling Deng[1]*, Yilin Liu[1]*, Kuo-En Chen[2], Huan Wei[1], Xiner Huang[1], Wanying Huang[1], Ping Zheng[1,3], Takashi Ueda[4], Richard D. Vierstra[2], Xiao Huang[1] and Faqiang Li[1,5,6]

[1]College of Life Sciences, South China Agricultural University, Guangzhou, 510642, China; [2]Department of Biology, Washington University in St. Louis, St Louis, MO 63130, USA; [3]School of Life Sciences, Huizhou University, Huizhou, 516007, China; [4]Division of Cellular Dynamics, National Institute for Basic Biology, Okazaki, Aichi, 444-8585, Japan; [5]State Key Laboratory for Conservation and Utilization of Subtropical Agro-Bioresources, South China Agricultural University, Guangzhou, 510642, China; [6]Guangdong Provincial Key Laboratory for the Development Biology and Environmental Adaptation of Agricultural Organisms, South China Agricultural University, Guangzhou, 510642, China

Authors for correspondence:
Faqiang Li
Email: fqli@scau.edu.cn

Xiao Huang
Email: xiaohuang@scau.edu.cn

Received: *9 February 2025*
Accepted: *4 July 2025*

New Phytologist (2025)
doi: 10.1111/nph.70418

Key words: Arabidopsis, ATG8, autophagosome–vacuole fusion, autophagy, nutrient recycling, Rab GTPase, vacuole.

Summary

- The ubiquitin-like protein ATG8 is a central component of the autophagy process and is required at multiple steps during both bulk and selective autophagy. Currently, our understanding of the roles of ATG8 in plants and the possible functional specialization of its family members is limited by genetic redundancy.
- Here, we employed clustered regularly interspaced short palindromic repeats (CRISPR)/CRISPR-associated (Cas)9 targeting technology to systematically inactivate all nine *Arabidopsis thaliana* ATG8 loci. Subsequent analyses of the resulting mutants revealed that, unlike mammalian ATG8 family members, which have distinct roles, *Arabidopsis* isoforms largely overlap in their functions controlling autophagic flux. Notably, combinatorial mutations have similarly impaired autophagy and misregulated proteomes much like other autophagy mutants.
- We further examined the functional redundancy of *Arabidopsis* ATG8s in late autophagy stages by investigating their interactions with Rab GTPase (RABG)3/RAB7 proteins. We found that all ATG8 representatives could interact with RABG3 proteins via ATG8-interacting motif–LC3-interacting region-docking site interfaces. Such interactions are crucial for RABG3 binding to the autophagosome membrane and probably for the fusion of autophagosomes with the vacuole. However, they are not necessary for endosomal trafficking.
- With this collection of multiple high-order *atg8* mutants, we provide a venue to selectively study the roles of individual ATG8 isoforms during both canonical and noncanonical autophagy in *Arabidopsis*.

Introduction

Autophagy is an intracellular catabolic pathway, which plays critical roles in maintaining cellular homeostasis, enabling metabolic recycling, promoting growth and development, and helping organisms overcome nutrient deprivation. During macroautophagy (refered to here as autophagy), cytoplasmic material is engulfed into double membrane-bound vesicles called autophagosomes, which then fuse with the lysosomes (metazoans) or the vacuoles (yeast and plants) for breakdown (Marshall & Vierstra, 2018; Nakatogawa, 2020; Qi *et al.*, 2021; Zhao *et al.*, 2021). Initially, it was thought that autophagy is a nonselective, bulk degradative process essential for survival under stress. However, studies in the last two decades have revealed that autophagy can also be highly selective for specific intracellular components, which are recruited to autophagosomes via dedicated receptors/adaptors (Johansen & Lamark, 2020).

The formation of autophagosomes depends on the sequential orchestration of a set of conserved autophagy-related (ATG) proteins (Nakatogawa, 2020). One of the central components of this autophagy machinery is the ubiquitin-like protein ATG8, which plays vital roles during most, if not all, steps of the autophagic process, including phagophore expansion, autophagosome closure and trafficking, fusion with a lysosome/vacuole, and selective cargo recruitment (Kriegenburg *et al.*, 2018). Similar to ubiquitin, ATG8 is modified by conjugation, in this case to the lipid phosphatidylethanolamine (PE) via its C-terminal glycine residue, and then recruited to the membranes of autophagic vesicles. Those bound to the rim and outer surface of the phagophore facilitate its growth by recruiting other core autophagy proteins

*These authors contributed equally to this work.

© 2025 The Author(s).
New Phytologist © 2025 New Phytologist Foundation.

(Xie *et al.*, 2008; Nakatogawa, 2020), and promote the autophagosome–lysosome/vacuole fusion by enrolling the core fusion machinery, including the regulator MONENSIN SENSITIVITY1 (MON1)–CALCIUM CAFFEINE ZINC SENSITIVITY1 (CCZ1) complex, soluble N-ethylmaleimide-sensitive factor attachment protein receptor (SNARE) proteins, and tethering factors (Itakura *et al.*, 2012; McEwan *et al.*, 2015; Gao *et al.*, 2018). By contrast, lipidated ATG8 decorating the inner membrane acts as a hub for recruiting autophagic receptors and/or cargoes during selective autophagy. These ATG8-interacting receptors/cargoes often contain one or more ATG8-binding sites, such as the ATG8-interacting motif/LC3-interacting region (AIM/LIR), which recognizes the LIR-docking site (LDS) in ATG8, or possibly the ubiquitin-interacting motif (UIM) proposed to bind an adjacent UIM-docking site (UDS) (Marshall *et al.*, 2019; Johansen & Lamark, 2020).

In addition to its essential roles, which are commonly described as 'canonical' functions, a growing number of studies in mammalian cells have found that ATG8 can be incorporated into divergent single-membrane vesicles that are involved in degradation or secretion, which act independently of canonical autophagy (Nieto-Torres *et al.*, 2021). Interestingly, recent studies have potentially uncovered such noncanonical routes in plants whereby ATG8 is translocated to swollen Golgi cisternae to aid in their reassembly after heat stress (Zhou *et al.*, 2023), and to the tonoplast to help maintain vacuolar integrity following cell wall damage (Zheng *et al.*, 2024; preprint; Julian *et al.*, 2025). Furthermore, ATG8 has been found to directly interact with the late endosome-resident transporter ABNORMAL SHOOT3 (ABS3) to facilitate its vacuolar degradation through a lipidation-independent process (Jia *et al.*, 2019).

Although highly conserved across eukaryotes, ATG8 has diversified from a single protein in fungi and algae to multiple isoforms in metazoans and seed plants (Kellner *et al.*, 2017). At least eight ATG8 isoforms have been identified in mammals, which can be divided into two subfamilies light chain3 (LC3) and GABA type A receptor-associated protein (GABARAP) based on their amino acid sequence homology and apparent subfunctionalization, as identified by genetic and interaction analyses. Similarly, ATG8 in seed plants is often encoded by small gene families with possible evidence of subfunctionalization; for example, *Arabidopsis thaliana* and rice (*Oryza sativa*) express nine and five ATG8 isoforms, respectively, with distinct expression patterns (Sláviková *et al.*, 2005; Xia *et al.*, 2011). The *Arabidopsis* isoforms can be further grouped phylogenetically into two clades. Clade I members (ATG8a-ATG8g) are more closely related to that in yeast and are synthesized with extra amino acids beyond the C-terminal glycine, thus requiring processing by the ATG4 protease to release the active polypeptide. By contrast, Clade II members (ATG8h and ATG8i) are more closely related to the animal relatives and lack this C-terminal extension, making them immediately available for lipidation (Kellner *et al.*, 2017).

Currently, full understandings of ATG8 in plants and the possible functional specialization of its family members are limited due to genetic redundancy. While numerous genetic analyses focusing on other components in the *Arabidopsis* conjugation machinery (e.g., ATG5, ATG7, ATG12, and ATG10), as well as on plants that overexpress ATG8, have shown that ATG8 and its lipidation are critical for plant growth, development, and survival under stress conditions (Doelling *et al.*, 2002; Thompson *et al.*, 2005; Phillips *et al.*, 2008; Chung *et al.*, 2010; Xia *et al.*, 2012; Wang *et al.*, 2016; Chen *et al.*, 2019; Fan *et al.*, 2020; Zhen *et al.*, 2021; Kanne *et al.*, 2022), how individual ATG8 isoforms and the Clade I and II variants act is unclear. Toward this goal, several studies have described high-order mutants. For example, Lan *et al.* (2024) reported that the simultaneous inactivation of *Arabidopsis ATG8h* and *ATG8i* led to enhanced resistance against the biotrophic fungal pathogen *Golovinomyces cichoracearum*, likely through specific interactions with the CLATHRIN LIGHT CHAIN (CLC) subunits 2 and 3, while simultaneous disruption of multiple rice *ATG8* loci was found to delay flowering, likely due to a block in the autophagy-mediated breakdown of the central flowering regulator Hd1 (Hu *et al.*, 2022). Additionally, by characterizing ATG8-interacting proteins, including SH3 DOMAIN-CONTAINING PROTEIN2 (SH3P2) (Zhuang *et al.*, 2013; Sun *et al.*, 2022), FREE1/FYVE1 (Zeng *et al.*, 2023), FYVE2 (also known as CFS1) (Kim *et al.*, 2022; Zhao *et al.*, 2022), and SAR1d (Zeng *et al.*, 2021), possible roles for specific ATG8 proteins in phagophore expansion, autophagosome closure, and maturation have emerged, strengthening the notion that diversity within the plant ATG8 family has expanded autophagic functionality/capacity.

One such expansion might be through the Rab GTPase RAB7 and its yeast counterpart Ypt7, which are essential for endocytic membrane trafficking from late endosome to lysosome/vacuole, and for the autophagosome–lysosome fusion (Guerra & Bucci, 2016). As triggered by the ATG8-binding guanine nucleotide exchange factor MON1-CCZ1 complex, RAB7/Ypt7 target to autophagosomes, and then interact with multiple downstream effectors to drive membrane fusion (Hegedűs *et al.*, 2016; Gao *et al.*, 2018; Zhao *et al.*, 2021). Similarly, plant RAB7 GTPases are recruited to prevacuolar compartments (PVCs) and activated by the MON1-CCZ1 complex to regulate vacuolar trafficking, vacuole biogenesis, and plant growth (Cui *et al.*, 2014; Singh *et al.*, 2014). However, the precise role(s) of RAB7 in plant autophagy and the manner in which it is recruited to autophagosomal membranes, possibly through ATG8, remain unclear.

To investigate the roles of ATG8 isoforms in plants, we used clustered regularly interspaced short palindromic repeats (CRISPR)/CRISPR-associated (Cas)9 technology to systematically inactivate all nine of the corresponding genes. Through their phenotypic analyses, we found that, unlike mammalian ATG8, in which the LC3 and GABARAP subfamilies act differentially at the early and late stages of autophagy, respectively, the *Arabidopsis* ATG8 proteins have overlapping roles in controlling autophagic flux. Combinatorial mutations of Clade I and Clade II isoforms showed severely impaired autophagy under nutrient starvation conditions. Additionally, we investigated the functional redundancy of *Arabidopsis* ATG8s at the late stages of autophagy by examining their interactions with Rab GTPase (RABG)3/RAB7 proteins and found that the representative ATG8s from all major clades/subclades could interact with

© 2025 The Author(s).
New Phytologist © 2025 New Phytologist Foundation.

14698137, 0, Downloaded from https://nph.onlinelibrary.wiley.com/doi/10.1111/nph.70418 by University Of British Columbia, Wiley Online Library on [01/09/2025]. See the Terms and Conditions (https://onlinelibrary.wiley.com/terms-and-conditions) on Wiley Online Library for rules of use; OA articles are governed by the applicable Creative Commons License

14698137, 0, Downloaded from https://nph.onlinelibrary.wiley.com/doi/10.1111/nph.70418 by University Of British Columbia, Wiley Online Library on [01/09/2025]. See the Terms and Conditions (https://onlinelibrary.wiley.com/terms-and-conditions) on Wiley Online Library for rules of use; OA articles are governed by the applicable Creative Commons License

RABG3 proteins through AIM-LDS interfaces. These interactions are essential for the association of RABG3 proteins with autophagosomes and likely for the autophagosome–vacuole fusion, but not for endosomal trafficking pathways. With the available collection of high-order mutations impacting ATG8 and RABG3, studying specific ATG8 isoforms during canonical and noncanonical autophagy in *Arabidopsis* is now possible.

Materials and Methods

Vector construction

For the constructions used for transient expression in *Arabidopsis* protoplasts, the coding sequences (CDS) of *SH3P2*, *NBR1*, *ABS3*, *RABG3f*, and several *ATG* genes (*ATG1a*, *ATG9*, *ATG14a*, *ATG5*, and *ATG8a*) were PCR-amplified using specific oligonucleotide primers (Supporting Information Table S1) and cloned into the pBI221 vector modified to either contain in-frame N-terminal green fluorecent protein (GFP) or mCherry tag, and expressed under the control of the *35S* promoter (Li *et al.*, 2022). The *pBI221-mCherry-RABG3f*^{mAIM1,2} construction was generated by PCR mutagenesis to introduce point mutations (F94A/L99A/F167A/I172A) in the AIM sequences of RABG3f, and cloned into the pBI221 vector with a mCherry tag. The Aleu-GFP construction was described previously (Cui *et al.*, 2017). The tonoplast marker mCherry-VAMP711 was obtained from Professor Liwen Jiang's lab.

To generate constructions for investigating RABG3-ATG8 protein interactions in tobacco (*Nicotiana benthamiana*) via luciferase (LUC) complementation imaging (LCI) assays, the CDS of *RABG3f*, *RABG3b*, *RABG3d*, *RABG3e*, *ATG8a*, *ATG8e*, and *ATG8h* were amplified and cloned in-frame into *pCAMBIA1300-nLUC* and *pCAMBIA1300-cLUC*, respectively (Chen *et al.*, 2008). The constitutively active (CA, Q67L), dominant-negative (DN, T22N), and various AIM-mutated variants of RABG3f, RABG3f(CA), RABG3f(DN), RABG3f^{mAIM1}, RABG3f^{mAIM2}, and RABG3f^{mAIM1,2} were generated from RABG3f-nLUC by PCR-based mutagenesis.

To generate transgenic plants co-expressing GFP-ATG8a and mCherry-RABG3f (or mCherry-RABG3f^{mAIM1,2}), their full-length CDSs were inserted into a modified *pCAMBIA1300* vector harboring two different expression cassettes for in-frame N-terminal fusion with GFP or mCherry tags expressed by the constitutive *AtUBQ10* promoter. The resulting constructions (*pUBQ10:mCherry-RABG3f-NOS-pUBQ10:GFP-ATG8a-NOS* and *pUBQ10:mCherry-RABG3f*^{mAIM1,2}*-NOS-pUBQ10:GFP-ATG8a-NOS*) were transformed into the *Agrobacterium tumefaciens* strain GV3101 and then introduced into sextuple *rabg3a,b,c,d,e,f* (*rabg3f-6m*; Ebine *et al.*, 2014) plants using the floral-dip method (Clough & Bent, 1998). Homozygous *rabg3-6m* plants carrying the transgene were identified in the T3 generation based on hygromycin resistance and confocal fluorescence microscopy.

Plant materials and growth conditions

The *A. thaliana* (L.) Heynh ecotype Col-0 was used as the wild-type (WT) in this study. The T-DNA insertion mutants *atg5-1* (Thompson *et al.*, 2005), *atg7-2* (Chung *et al.*, 2010), *gfs9-3* (Ichino *et al.*, 2014), and *rabg3-6m* (Ebine *et al.*, 2014), as well as transgenic plants expressing the *p35S:GFP-ATG8a* (Thompson *et al.*, 2005), *ProUBQ10:GFP-ATG8a* (Shin *et al.*, 2014), and *pUBQ10:mCherry-RabG3f* (Geldner *et al.*, 2009) transgenes, all in the Col-0 background, were described previously. The *gfs9-4/tt9* mutant (Ichino *et al.*, 2014) was in the Landsberg *erecta* (L*er*) background. Fluorescent protein expression cassettes *p35S:GFP-ATG8a* and *pUBQ10:mCherry-RABG3f* were introgressed into the *gfs9-4/tt9* mutant by crossing. Segregants containing the Col-0 allele of *GFS9* were used as controls. To determine the effect of the *RABG3* mutations on autophagic activity, a construction harboring *ProUBQ10:GFP-ATG8a* (hygromycin resistance; Shin *et al.*, 2014) was transformed into the *rabg3-6m* lines by the floral-dip method. Homozygous *rabg3-6m* plants carrying the transgene were identified in the T3 generation based on hygromycin resistance and confocal fluorescence microscopy.

Unless otherwise indicated, all *Arabidopsis* seeds were surface-sterilized by the vapor-phase method and stratified in water for 2 d at 4°C in the dark before sowing on Murashige and Skoog (MS) solid medium supplemented with 1% (w/v) sucrose (Suc). Plants were grown at 22°C under a long-day (LD; 16 h : 8 h, light : dark) photoperiod for 10 d before being transferred to soil for further growth. For senescence assays, plants were grown in soil under LD conditions for 7 wk or under a short-day (SD; 8 h : 16 h, light : dark) photoperiod at 22°C for 10 wk.

For N starvation treatments, 7-d-old seedlings grown on MS solid medium with 1% (w/v) Suc were transferred to MS liquid medium with or without nitrogen. Seedlings were grown under continuous white light irradiation for the indicated times before imaging and measurement of Chl content as previously described (Suttangkakul *et al.*, 2011). Alternatively, seeds were germinated on solid MS medium containing 1% (w/v) Suc and 1.4% (w/v) agar with or without nitrogen and grown vertically. After 7 d, the seedlings were imaged, and root lengths were measured as described previously (Xiao *et al.*, 2020).

For carbon starvation, 2-wk-old seedlings grown on solid MS medium without Suc were wrapped in aluminum foil and kept in the dark for the indicated times before recovery under LD conditions. After 2 wk, seedlings were imaged, and survival rates were determined as previously described (Suttangkakul *et al.*, 2011). Alternatively, seedlings were grown for 7 d on solid MS medium containing 1% (w/v) Suc. Those of uniform size were transferred to solid MS medium without Suc and grown vertically in continuous darkness for the indicated time before imaging and Chl measurements.

Generation of the *atg8* nonuple mutants

The constructions for CRISPR mutagenesis were generated using an egg cell-specific promoter-controlled CRISPR/Cas9 genome editing system (Xing *et al.*, 2014; Wang *et al.*, 2015). Three CRISPR/Cas9 vectors were engineered to selectively disrupt the *ATG8abcd*, *ATG8efg*, and *ATG8hi* loci using guide RNAs

© 2025 The Author(s).
New Phytologist © 2025 New Phytologist Foundation.

specific for the target *ATG8* genes as designed by the CRISPR-GE website (http://skl.scau.edu.cn/) and cloned into the pHEE401E vector. Information related to the cloning primers, the arrangement of the sgRNAs in three CRISPR/Cas9 vectors, and the sequences of the CRISPR plasmids are available in Table S1 and Notes S1. The generated constructions were then introduced into the WT Col-0 plants by the *A. tumefaciens*-mediated floral-dip method. The resulting T1 transformants were selected by hygromycin resistance, and positive plants were transferred to soil after 2 wk. Mutations were identified by PCR amplification of the genomic regions encompassing the DNA target sites and confirmed by DNA sequence analysis (see Table S1, for PCR primer sequences). In the next generation, mutants were further confirmed by PCR and DNA sequencing to identify homozygous mutants absent of the hygromycin resistance and CRISPR/Cas9 vector sequences. After obtaining homozygous plants free of these loci, the CRISPR/Cas9 constructions targeting *ATG8abcd* and *ATG8hi* were introduced into the *atg8efg* triple mutant (*atg8-3m*) to generate the *atg8efghi* quintuple (*atg8-5m*) and the *atg8abcdefg* septuple mutants (*atg8-7m*), respectively. The *atg8abcdefghi* nonuple mutant (*atg8-9m*) was then generated using a CRISPR/Cas9 construction to simultaneously inactivate *ATG8h and ATG8i* in hygromycin-sensitive Cas9-free homozygous *atg8-7m* plants.

Transient expression in *Arabidopsis* protoplasts

The *Arabidopsis* leaf protoplast preparation and transient expression were performed according to a standard procedure (Yoo *et al.*, 2007). Briefly, confocal images were collected at 12–16 h or at the indicated times. To detect autophagic bodies in protoplasts, 1 μM concanamycin (ConA) (BVT-0237-M001; AdipoGen Life Sciences, San Diego, CA, USA) or an equivalent volume of dimethyl sulfoxide (DMSO) was added to the protoplasts for 12 h before observation.

Fluorescence confocal microscope imaging and analysis

Fluorescence cell images were collected using a Leica Stellaris 5 confocal microscope (Leica, Wetzlar, Germany). Confocal imaging of stable transgenic lines expressing GFP-ATG8a in WT and *rabg3-6m* and *gfs9-4* mutant backgrounds was performed as described previously (Suttangkakul *et al.*, 2011; Huang *et al.*, 2019). Briefly, 6-d-old seedlings grown on nitrogen-containing solid MS medium were transferred to either fresh nitrogen-rich medium or nitrogen-deficient medium supplemented with 1 μM ConA for the indicated time before image capture of root cells. To acquire the GFP signal, a 488-nm laser was used for excitation, and fluorescence was detected in the range of 490–540 nm. To image the co-expression of the GFP and mCherry reporters in leaf protoplasts and the root cells of stable transgenic lines, excitation wavelengths of 488 nm for GFP and 543 nm for mCherry were used alternately in the multitrack mode of the microscope with line switching. Quantitative analyses of the confocal microscopic images were conducted in ImageJ (https://imagej.nih.gov/) as described by Kim *et al.* (2022).

Luciferase complementation imaging assays

Interactions between RABG3 and ATG8 were investigated by luciferase complementation imaging (LCI) assays as described previously (Chen *et al.*, 2008). Briefly, different combinations of *RABG3* and *ATG8* constructions or empty vectors were introduced into the *A. tumefaciens* strain GV3101 and then co-infiltrated into tobacco leaves. The plants were immediately cultured in the dark for 16 h followed by exposure to LD conditions for an additional 2 d at 23°C. The infiltrated leaves were further infiltrated with 500 μM D-luciferin, and the resulting luminescence signals were captured using a low-light cooled charge-coupled device camera (Night owl LB985; Berthold Technologies, Bad Wildbad, Germany). After observation, the infiltrated leaves were collected and examined for the expression of nLUC- and cLUC-fusion proteins by immunoblotting with anti-LUC antibodies.

GST pull-down assays

GST-ATG8e was synthesized in *Escherichia coli* BL21 (DE3) after induction with 1 mM isopropyl-β-D-thiogalactoside (IPTG) for 16 h at 16°C. Total *E. coli* proteins were then extracted and incubated with Glutathione Sepharose beads (C650031; Sangon Biotech Co. Ltd., Shanghai, China) to enrich for the fusion. For the pull-down analysis, the GFP-nLUC, RABG3f-nLUC, and RABG3f^{mAIM1,2}-nLUC proteins were individually expressed in tobacco leaves by agroinfiltration of the vectors. After 3 d, *c.* 500 mg of infiltrated leaves was harvested and homogenized with 2 ml of lysis buffer (50 mM Tris–HCl (pH 7.4), 150 mM NaCl, 1 mM $MgCl_2$, 20% glycerol, 0.2% NP-40, and 1× protease inhibitor cocktail (04693132001; Roche)). Cell lysates were clarified twice by centrifugation at 13 000 ***g*** for 10 min at 4°C and then incubated with GST-ATG8e-bound beads for 1 h at 4°C. The beads were washed five times with 1 ml of wash buffer (140 mM NaCl, 2.7 mM KCl, 10 mM Na_2HPO4, and 1.8 mM KH_2PO4 (pH 7.4)) for 1 min each time. Proteins bound to the beads were released in SDS-PAGE sample buffer (100 mM Tris–HCl (pH 6.8), 4% (w/v) SDS, 0.2% (w/v) bromophenol blue, and 20% (v/v) glycerol) by heating the mixture to 95°C for 5 min before use in immunoblot assays.

Pollen analyses

Pollen germination *in vitro* was performed as described (Liu *et al.*, 2020). To detect pollen viability, fresh anthers from mature flowers were collected and mounted with 50 μl of Alexander stain solution (G3050; Solarbio Science & Technology Co. Ltd., Beijing, China) on glass microscope slides. The slides were incubated at 4°C for 5–10 h and then observed with a microscope (Leica DM2500; Leica Microsystems, Wetzlar, Germany). For 4',6-diamidino-2-phenylindole (DAPI) staining, mature pollen grains were isolated from freshly opened flowers by vortexing and stained with 1 μg ml^{-1} DAPI solution (E607303; Sangon Biotech) for 1 h. Then, the grains were observed using a confocal laser microscope (Stellaris 5; Leica).

© 2025 The Author(s).
New Phytologist © 2025 New Phytologist Foundation.

14698137, 0, Downloaded from https://nph.onlinelibrary.wiley.com/doi/10.1111/nph.70418 by University Of British Columbia, Wiley Online Library on [01/09/2025]. See the Terms and Conditions (https://onlinelibrary.wiley.com/terms-and-conditions) on Wiley Online Library for rules of use; OA articles are governed by the applicable Creative Commons License

14698137, 0, Downloaded from https://nph.onlinelibrary.wiley.com/doi/10.1111/nph.70418 by University Of British Columbia, Wiley Online Library on [01/09/2025]. See the Terms and Conditions (https://onlinelibrary.wiley.com/terms-and-conditions) on Wiley Online Library for rules of use; OA articles are governed by the applicable Creative Commons License

Protein extraction and immunoblot assays

To detect the various ATG proteins and GFP/mCherry-tagged fusions by immunoblot assays, 100 mg of seedlings was homogenized in 200 µl of 2× SDS-PAGE sample buffer followed by heating at 95°C for 5 min. The plant lysates were clarified twice by brief centrifugation at 14 000 ***g*** for 10 min at room temperature, and the resulting supernatants were subjected to SDS-PAGE and immunoblot analysis. Antibodies against the autophagy-related 1a, a serine/threonine-protein kinase (ATG1a) (Suttangkakul *et al.*, 2011), ATG5, ATG8a (Thompson *et al.*, 2005), PBA1 (Smalle *et al.*, 2002), GFP (ab290; Abcam, Cambridge, UK), mCherry (B1153; Biodragon, Beijing, China), GST (B1007; Biodragon), and LUC (L0159; Sigma-Aldrich) were previously described. Protein levels were quantified by ImageJ according to Kim *et al.* (2022).

Protein sample preparation for MS analysis

To prepare seedling samples for MS analysis, sterilized WT and *atg* mutant seeds were germinated and grown under continuous light in 250-ml flasks containing 50 ml of liquid MS medium supplemented with 1% Suc for 7 d. For nitrogen starvation, the plants were transferred to liquid MS medium with or without nitrogen for 3 d. For fixed-carbon starvation, the plants were transferred to liquid MS medium with or without Suc for 2 d, during which time the flasks containing carbon-starved plants were covered with aluminum foil. Seedlings were harvested and homogenized in liquid nitrogen and extraction buffer (50 mM HEPES (pH 7.5), 5 mM Na_2EDTA, 2 mM DTT, and 1× protease inhibitor cocktail). Total extracted proteins were precipitated using a 4 : 1 : 3 (v/v) methanol : chloroform : water mixture, collected by centrifugation, washed once with methanol, and then lyophilized to dryness. The precipitates were then resuspended in 100 µl of 8 M urea and reduced with 10 mM dithiothreitol for 1 h at room temperature. For trypsin digestion, 100 µg of protein was alkylated with 20 mM iodoacetamide for 1 h, and the reaction was quenched with 20 mM dithiothreitol. The sample was diluted with 900 µl of 25 mM ammonium bicarbonate to reduce the urea concentration below 1 M and digested overnight at 37°C with sequencing grade-modified porcine trypsin (Promega) at a trypsin : protein ratio of 1 : 50. The resulting peptides were lyophilized to a volume of < 50 µl, acidified with 10% trifluoroacetic acid to a pH below 3.0, and desalted and concentrated using Pierce C18 tips (Thermo Fisher Scientific, Waltham, MA, USA) according to the manufacturer's instructions. Peptides were eluted in 50 µl of 75% acetonitrile and 0.1% acetic acid, lyophilized again, and resuspended in 15 µl of 5% acetonitrile and 0.1% formic acid for LC-MS/MS analysis.

Tandem mass spectrometric analysis and data processing

Full mass spectrometric (MS/MS) scans were performed in the mass range of 380–1500 *m/z* at a resolution of 70 000, with an automatic gain control target of 3×10^6 and a maximum injection time of 200 ms. Data-dependent acquisition was applied to fragment the top 15 most intense peaks using high-energy collision-induced dissociation at a normalized collision energy of 28. An intensity threshold of 4×10^4 counts and an isolation window of 3.0 *m/z* were applied. Precursor ions with unassigned charges or charges between +1 and +7 were excluded. MS/MS scans were collected at a resolution of 17 500, with an automated gain control (AGC) target of 2×10^5 and a maximum fill time of 300 ms. Dynamic exclusion was performed with a repeat count of 2 and an exclusion duration of 30 s, while the minimum MS ion count to trigger tandem MS was set to 4×10^3 counts. Raw sequencing data were deposited in the PRoteomics IDEntifications Database (PRIDE; accession no.: PXD059803).

The resulting MS/MS spectra were analyzed using Proteome Discoverer (v.2.5; Thermo Fisher Scientific) against the *A. thaliana* Col-0 proteome database (Araport11_pep_20220914) downloaded from The Arabidopsis Information Resource (TAIR) (http://www.tair.com/). Peptide assignments were performed using SEQUEST HT with the following parameters: trypsin digestion allowing a maximum of two missed cleavages, a minimum peptide length of six residues, a precursor mass tolerance of 10 ppm, and a fragment mass tolerance of 0.02 Da. Carbamidomethylation of cysteines and oxidation of methionines were specified as static and dynamic modifications, respectively. False discovery rates (FDRs) of 0.01 (high confidence) and 0.05 (medium confidence) were used to validate peptide spectral matches. Label-free quantification based on MS1 precursor ion intensities was performed in Proteome Discoverer with a minimum Quan value threshold set to 0.0001 for unique peptides; the '3 Top N' peptides were used for area calculation. All genotypes and treatments were analyzed by four biological replicates, each with two technical replicates.

Protein abundances were normalized using the values of the 150 least variable proteins (determined by the SD : average ratio) across samples for each run (McLoughlin *et al.*, 2018). Protein abundances were further adjusted based on protein content per weight of plant tissue for each biological replicate. Normalization was validated by comparing the abundances of tubulin peptides (Figs 3a, S7). Standardized data were used to filter proteins, each of which must be present in at least one technical replicate of each of the four biological replicates for at least one genotype. To generate volcano plots, data were first transformed to Log_2 values, with missing value imputation and statistical calculations conducted in the Perseus software, followed by visualization using GraphPad Prism (v.10). Statistic differences between the *atg* mutants and WT were determined based on four biological replicates using Student's *t*-test (Log_2 FC ≥ 1 or ≤ -1, $P \leq 0.05$). Gene Ontology (GO) analyses were performed using the *Arabidopsis* profile database in g:Profiler v.3.10.178 as part of the ELIXIR INFRASTRUCTURE package (http://biit.cs.ut.ee). The GO annotation categories shown here were selected based on their uniqueness, *P*-values of significance, and degrees of completeness.

Results

Multigene inactivation of *Arabidopsis ATG8* genes

The *Arabidopsis* ATG8 protein family consists of nine members (ATG8a to ATG8i), which can be divided into two major clades

© 2025 The Author(s).
New Phytologist © 2025 New Phytologist Foundation.

based on their sequence homology and genomic structure (Kellner *et al.*, 2017). Clade II includes the ATG8h and ATG8i isoforms, whereas Clade I encompasses ATG8a-g, which can be further split into two subclades (I-1, ATG8a-d; I-2, ATG8e-g) by sequence homology (Kellner *et al.*, 2017). To investigate the significance of the various ATG8 isoforms during autophagy, we used an egg cell-specific CRISPR/Cas9 mutagenic approach to systematically edit each of the nine *ATG8* genes (Wang *et al.*, 2015). Three CRISPR/Cas9 vectors were constructed to selectively target the CDSs of the *ATG8* loci within subclade I-1 (*ATG8a-d*), subclade I-2 (*ATG8e-g*), and Clade II (*ATG8h-i*), respectively, in ways that should abrogate the expression of the full-length ATG8 polypeptides (Fig. 1a,b; Notes S1). Through *A. tumefaciens*-mediated, floral-dip transformation of WT Col-0 plants, first-generation *Arabidopsis* seedlings were obtained that harbored specific mutations in the *ATG8e-g loci*. Additional CRISPR/Cas9 vectors were then introduced to further inactivate the *ATG8a-d* and *ATG8h-i* loci in the Cas9-free *atg8-3m* to generate the *atg8-5m* and the *atg8-7m*, respectively. Finally, we generated an *atg8-9m* in the Cas9-free *atg8-7m* background using a CRISPR/Cas9 construction to disrupt *ATG8h* and *ATG8i*. Mutations in the double (*atg8hi*, also referred to as *atg8-2m*), triple, quadruple (*atg8abcd*, also referred to as *atg8-4m*), quintuple, septuple, and nonuple mutants were confirmed by PCR and DNA sequencing as shown in Fig. S1. Based on nucleotide sequence analyses, all the mutations in the impacted *ATG8* loci were expected to compromise the expression of the corresponding genes.

To define how different *atg8* mutations affected the ATG8 protein accumulation, we performed an immunoblot analysis of total protein extracts from seedlings using antibodies raised against the recombinant *Arabidopsis* ATG8a protein, which also readily detects the most divergent ATG8 isoform, ATG8i (Doelling *et al.*, 2002). As shown in Fig. 1(c), ATG8 protein levels remained high in protein extracts obtained from *atg8-2m*, *atg8-3m*, *atg8-4m*, and *atg8-5m* seedlings, whereas the levels of detectable ATG8 became significantly reduced in homozygous *atg8-7m* lines. In the nonuple *atg8-9m* seedlings, only trace amounts of ATG8 were possibly detected, which could represent a truncated remnant of one or more ATG8 isoforms, the most likely being mutated ATG8g derived from the CRISPR/Cas9 editing (Fig. 1b,c). In any case, the nonuple mutant expressed little to none of the full-length ATG8 polypeptides.

As an indirect measure of the effects of the *atg8* mutations on autophagy, we measured the levels of ATG1, which is not only a regulator but also a cargo of autophagic degradation whose levels rise in various *atg* mutant backgrounds (Suttangkakul *et al.*, 2011). In *atg8-7m* and *atg8-9m* seedlings, ATG1 levels were constitutively upregulated as compared with the WT, similar to that observed for the *atg7-2* mutant, suggesting that ATG1 degradation, and by inference overall autophagy, was substantially impaired in both backgrounds with the stronger effect seen in the *atg8-9m* lines as predicted (Fig. 1c). By contrast, the *c.* 48-Da ATG12–ATG5 conjugate, which is required for ATG8 lipidation but not for free ATG5, was readily detected using anti-ATG5 antibodies in all the *atg8* mutant backgrounds, similar to that seen in the WT. Notably, the amount of free ATG5 increased subtly in *atg8-9m* seedlings (Figs 1c, 7f), suggesting that a complete removal of *ATG8* genes somehow affects the assembly of ATG12–ATG5.

To further understand how our collection of *atg8* mutants compromises autophagy in general, we used protoplast transient assays to investigate whether the mutations alter the subcellular localizations of other ATG proteins, the selective autophagy receptor NBR1, or the multidrug and toxic compound extrusion (MATE) transporter ABS3. Unlike the WT protoplasts, no GFP-ATG1a- and GFP-ATG14-decorated puncta were seen in *atg7-2* or *atg8-9m* cells treated with the v-ATPase inhibitor ConA, which stabilizes autophagic bodies (Fig. S2a,b), consistent with the notion that both ATG1 and ATG14 need ATG8 for association with autophagosomes/autophagic bodies (Suttangkakul *et al.*, 2011; Liu *et al.*, 2020). Conversely, the subcellular distributions of other ATG components, including ATG9, SH3P2, and ATG5, were unperturbed in *atg7-2* or *atg8-9m* protoplasts compared with those seen with WT, implying ATG8-independent binding to the vesicles (Fig. S2c).

For NBR1-GFP, its fluorescence appeared as punctate spots in the cytoplasm of all mutant protoplasts, including *atg7-2* and *atg8-9m* cells before ConA treatment (Fig. S3a). However, after ConA treatment, NBR1-GFP puncta were now readily detected in the vacuolar lumen of WT, *atg8-2m*, *atg8-3m*, *atg8-4m*, *atg8-5m*, and *atg8-7m* cells, but not in *atg7-2* or *atg8-9m* cells (Fig. 1d). Cotransformation of NBR1-GFP with the tonoplast marker mCherry-VAMP711 further confirmed the deficiency of NBR1 transport to the vacuole in the *atg8-9m* mutant (Fig. S3b), implying that at least some ATG8 is required for the encapsulation of this cargo receptor. For ABS3-GFP, we detected endosomal ABS3-GFP puncta in all DMSO-treated protoplasts and found punctate ABS3-GFP signals in the vacuoles of ConA-treated WT and *atg7-2* protoplasts (Fig. S4), consistent with a previous study showing that the vacuolar trafficking of ABS3-GFP is independent of the ATG8 conjugation machinery (Jia *et al.*, 2019). However, the deposition of ABS3-GFP in the vacuole was completely abolished in the *atg8-9m* background, as ABS3-GFP maintained a predominantly endosomal distribution at the cell periphery (Fig. S4). Taken together, these results demonstrate that the *atg8-9m* seedlings behave as a functionally null *atg8* mutant in which both non-selective autophagy and selective autophagy, and the autophagy-independent proteolysis of ABS3 are severely impaired. Furthermore, given that the lesser level mutant combinations specifically impacting members of the I-1 and I-2 subclades from Clade I (*atg8-4m* and *atg8-3m* eliminating *ATG8abcd*, *and ATG8efg*, respectively), and both members of Clade II (ATG8h,i) did not selectively increase ATG1 levels nor impacted the intracellular localizations of ATG1 and ATG14 (Figs 1c–f, S2a,b), we concluded that the various *Arabidopsis* ATG8 isoforms are functionally redundant, at least with regard to canonical autophagy.

Plants lacking ATG8 senesce early and are hypersensitive to nutrient starvation

To determine how a lack of ATG8 might compromise *Arabidopsis* plants phenotypically, we monitored their growth and development under nitrogen- and fixed carbon-rich and -depleted conditions

© 2025 The Author(s).
New Phytologist © 2025 New Phytologist Foundation.

14698137, 0, Downloaded from https://nph.onlinelibrary.wiley.com/doi/10.1111/nph.70418 by University Of British Columbia, Wiley Online Library on [01/09/2025]. See the Terms and Conditions (https://onlinelibrary.wiley.com/terms-and-conditions) on Wiley Online Library for rules of use; OA articles are governed by the applicable Creative Commons License

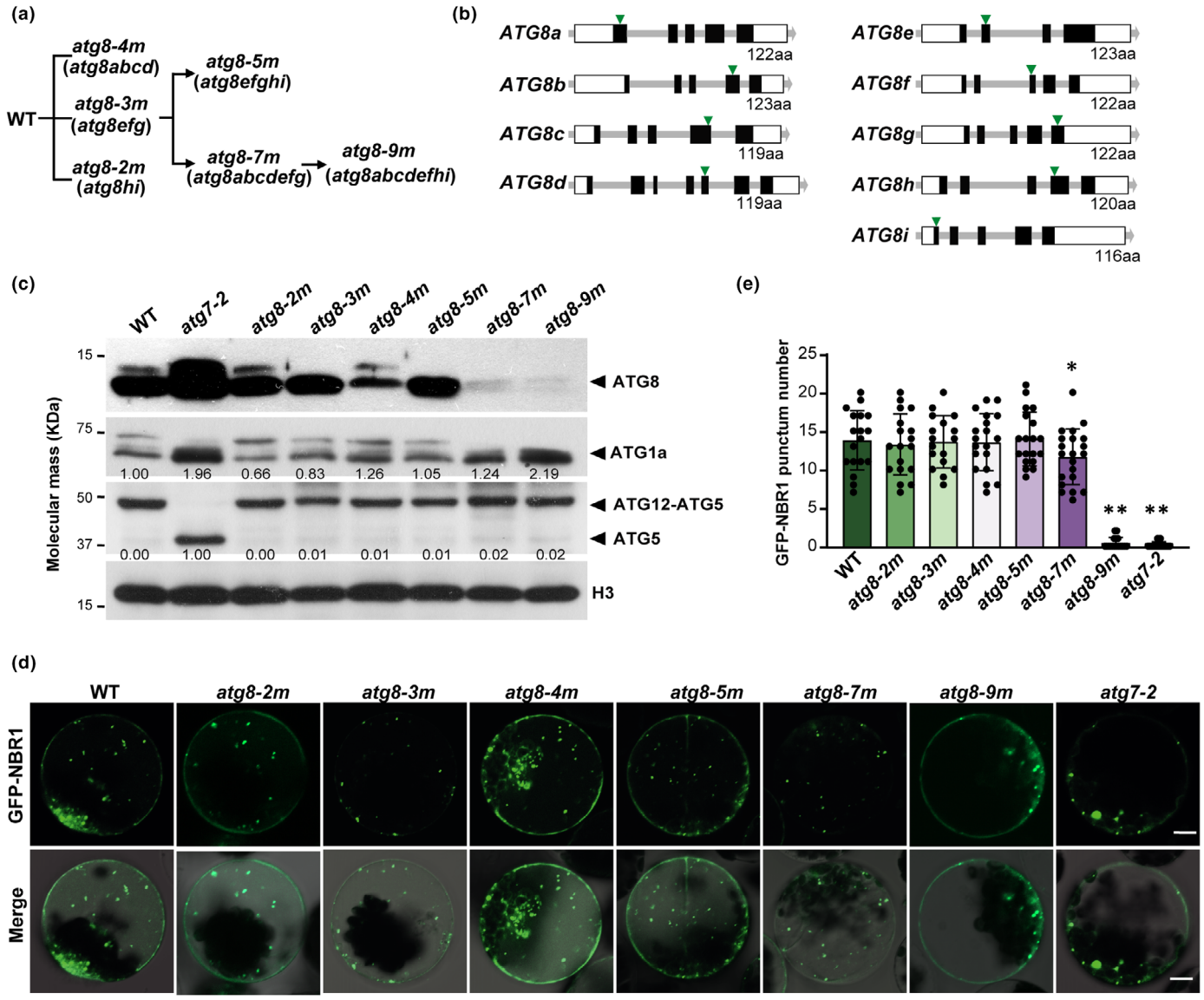

Fig. 1 Generation of *Arabidopsis atg8* nonuple mutants. (a) Generation of *Arabidopsis atg8* nonuple mutants. Three clustered regularly interspaced short palindromic repeats (CRISPR)/CRISPR-associated (Cas)9 constructions targeting *ATG8abcd*, *ATG8efg*, or *ATG8hi* were constructed and transformed into wild-type (WT) Col-0 to generate *atg8abcd* quadruple mutant (*atg8-4m*), *atg8efg* triple mutant (*atg8-3m*), and *atg8hi* double mutant (*atg8-2m*), respectively. Subsequently, CRISPR/Cas9 constructions targeting *ATG8abcd* and *ATG8hi* were transferred into the *atg8-3m* mutant to generate the *atg8efghi* quintuple mutant (*atg8-5m*) and the *atg8abcdefg* septuple mutant (*atg8-7m*), respectively. To generate *atg8* nonuple mutants, a CRISPR/Cas9 construction targeting *ATG8hi* was transferred into the *atg8-7m* mutant. (b) Diagram illustrating the *ATG8* genes and the selected target sites. Exons are shown as black boxes, 5′-untranslated region (5′-UTR), 3′-UTR as white boxes, and sgRNA target sites as green triangles. (c) Immunoblot detection of multiple ATG proteins from WT, *atg7-2*, and various *atg8* mutants using antibodies against ATG8, the autophagy-related 1a, a serine/threonine-protein kinase (ATG1a), and ATG5, respectively. Antibody against H3 was used as a loading control. Numbers below bands indicate the ATG1a/H3 or free ATG5/H3 ratios in the label lanes. For ATG1a/H3 ratios, the WT ratio is normalized to 1.0. For free ATG5/H3 ratios, the ratios of WT and *atg7-2* are normalized to 0.0 and 1.0, respectively. (d) Effects of different *atg8* mutations on the vacuolar transport of green fluorescent protein (GFP)-NBR1. Leaf protoplasts of WT, *atg7-2*, or various *atg8* mutants were transformed with the GFP-NBR1 construct and treated with 1 μM concanamycin A for 12–14 h before confocal imaging analysis. Bars, 10 μm. (e) Quantification of the number of vacuolar GFP-NBR1 puncta per 800 μm^2, using images (n = 18–22) similar to those shown in (d). Data are presented as mean ± SD Asterisked columns represent *atg8* mutants that are significantly different from WT, according to Student's *t*-test. *$0.01 < P < 0.05$; **$P < 0.01$.

(Huang *et al.*, 2019) along with mutants missing ATG5 and ATG7 essential for ATG8 lipidation. Similar to *atg5-1* and *atg7-2* plants (Thompson *et al.*, 2005; Chung *et al.*, 2010), the septuple *atg8-7m* and nonuple *atg8-9m* plants germinated and grew normally in nutrient-rich soil under glasshouse conditions (Fig. S5). Most of the pollens produced by *atg8-7m* and *atg8-9m* mutants were viable, as judged by vital staining with Alexander's stain (Fig. S6c). However, their pollen germination rates were

© 2025 The Author(s).
New Phytologist © 2025 New Phytologist Foundation.

14698137, 0, Downloaded from https://nph.onlinelibrary.wiley.com/doi/10.1111/nph.70418 by University Of British Columbia, Wiley Online Library on [01/09/2025]. See the Terms and Conditions (https://onlinelibrary.wiley.com/terms-and-conditions) on Wiley Online Library for rules of use; OA articles are governed by the applicable Creative Commons License

lower than those of the WT and the lesser order *atg8* mutants (*atg8-2m*, *atg8-3m*, *atg8-4m*, and *atg8-5m*) as measured by an *in vitro* germination assay (Fig. S6e,f). Moreover, seed formation was partially compromised in the *atg8-7m* and *atg8-9m* mutants, as well as in the *atg7-2* mutant (Fig. S6g,h), which is consistent with the previous observations in the *atg5* and *atg7* mutants (Yan

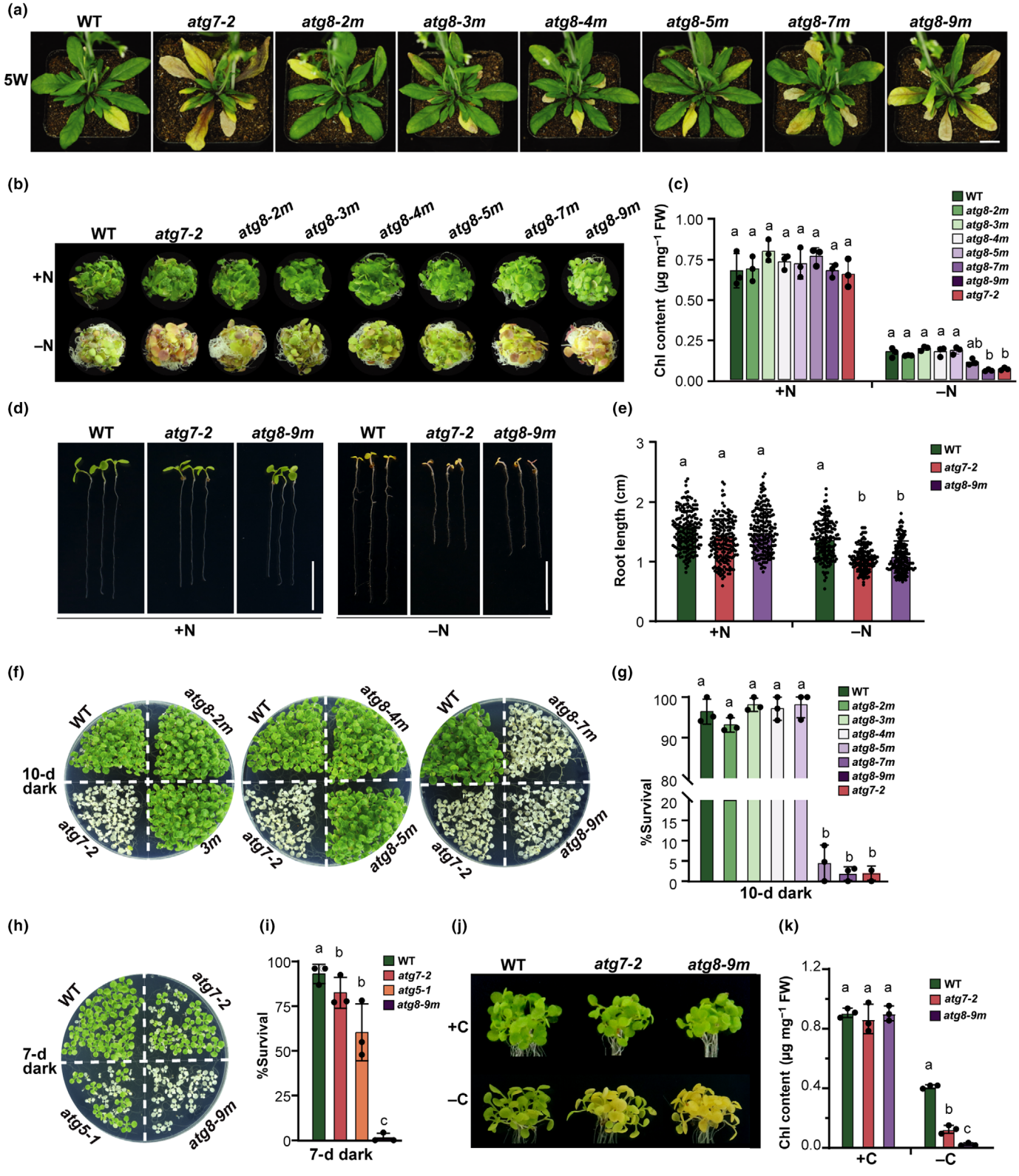

© 2025 The Author(s).
New Phytologist © 2025 New Phytologist Foundation.

14698137, 0, Downloaded from https://nph.onlinelibrary.wiley.com/doi/10.1111/nph.70418 by University Of British Columbia, Wiley Online Library on [01/09/2025]. See the Terms and Conditions (https://onlinelibrary.wiley.com/terms-and-conditions) on Wiley Online Library for rules of use; OA articles are governed by the applicable Creative Commons License

14698137, 0, Downloaded from https://nph.onlinelibrary.wiley.com/doi/10.1111/nph.70418 by University Of British Columbia, Wiley Online Library on [01/09/2025]. See the Terms and Conditions (https://onlinelibrary.wiley.com/terms-and-conditions) on Wiley Online Library for rules of use; OA articles are governed by the applicable Creative Commons License

Fig. 2 Phenotypic analyses of *Arabidopsis atg8* mutants. The various homozygous *atg8* mutants, the autophagy mutants *atg5-1* and *atg7-2*, and the wild-type (WT) Col-0 were included for comparisons. (a) Accelerated senescence. Plants were grown on soil at 22°C under a long-day (LD) photoperiod (16 h : 8 h, light : dark) for 5 wk. Bar, 1 cm. (b) Enhanced sensitivity to nitrogen starvation. Seeds were germinated in 1× Murashige and Skoog (MS) liquid medium and grown under constant white light conditions for 1 wk, and then transferred to either fresh MS (+N) or nitrogen-deficient (–N) liquid medium for an additional 1 wk. (c) Total Chl content of the plants shown in (b). Data are presented as mean ± SD (n = 3 biological replicates, 80–120 seedlings per genotype in each independent experiment). (d) Short primary root phenotype of *atg8-9m* in response to nitrogen deficiency. Seeds were germinated and grown vertically on MS medium with (+N) or without nitrogen (–N) under LD conditions for 1 wk. Bars, 1 cm. (e) Quantification of root length of the plants shown in (d). Data are presented as mean ± SD (n = 3 biological replicates, > 50 seedlings per genotype in each independent experiment). (f, h) Enhanced sensitivity to fixed-carbon starvation. Seedlings were grown under an LD photoperiod on MS solid medium without sucrose (–C) for 2 wk, transferred to darkness for 10 d (f) or 7 d (h), and then allowed to recover under LD conditions for 12 d. (g, i) Quantification of the effects of fixed-carbon starvation based on seedling survival after 10 d (f) or 7 d (h) in darkness followed by 12 d in LD. Data are presented as mean ± SD (n = 3 biological replicates, 60–120 seedlings per genotype in each independent experiment). (j) Senescence phenotypes of the *atg8-9m* after dark treatment. Seedlings were germinated and grown on ½MS solid medium with 1% sucrose under LD conditions for 1 wk, then transferred to ½MS medium without sucrose (–C) and grown vertically in the dark for another 7 d. (k) Total Chl content of the plants shown in (j). Data are presented as mean ± SD (n = 3 biological replicates, 80–120 seedlings per genotype in each independent experiment). Different letters in (c, e, g, i, k) indicate significant differences (P < 0.05) as determined using two-way ANOVA followed by Tukey's multiple comparison test.

et al., 2024). Similar to *atg5-1* and *atg7-2* plants, *atg8-7m* and *atg8-9m* plants also prematurely senesced when grown under LD conditions with early leaf yellowing seen as soon as 5 wk after planting. This yellowing occurred *c.* 1.5 wk earlier than that seen for the WT and the lesser order *atg8* mutants, implying that this senescence phenotype requires the inactivation of most, if not all *ATG8* loci (Fig. 2a).

We next challenged the *atg8* mutants with nitrogen- and fixed-carbon-limiting conditions to assess their sensitivity to nutrient stress. Similar to *atg7-2* seedlings, *atg8-9m* plants grew poorly and displayed stunted root growth, and the rosettes became strongly chlorotic when grown without nitrogen (Fig. 2b,e). Under fixed-carbon starvation, both *atg8-7m* and *atg8-9m* plants also grew poorly relative to the WT; in fact, nearly all of the mutants died after 10 d of darkness as judged by severe bleaching on the cotyledons and first true leaves, while only 4–7% of the WT plants and lesser order *atg8* mutants did so (Fig. 2f,g). Strikingly, *atg8-9m* seedlings showed an even higher sensitivity to fixed-carbon starvation than the *atg5-1* and *atg7-2* mutants; after 7 d in darkness, very few of the *atg8-9m* mutants survived as compared with 62% survival for *atg5-1* and 81% for *atg7-2* seedlings, which resumed growth after returning to fixed-carbon-replete conditions (Fig. 2h, i). This increased sensitivity was also demonstrated through a shorter fixed-carbon starvation treatment, in which light-grown 7-d-old seedlings were transferred to ½MS medium without Suc and kept in darkness (Jia *et al.*, 2019). Compared with WT and *atg7-2* seedlings, the *atg8-9m* seedlings displayed greatly accelerated senescence (Fig. 2j,k). Taken together, our phenotypic data with the lesser order *atg8* mutants and the complete inactivation of all nine *ATG8* loci agreed with the biochemical analyses and strongly suggest that the nine ATG8 isoforms are functionally redundant in *Arabidopsis* and that most, if not all, canonical autophagic activity is completely absent in the *atg8-9m* mutant background, as in other mutants that abrogate ATG8 lipidation.

atg8 Nonuple mutant substantially altered the *Arabidopsis* proteome after nitrogen and fixed-carbon starvations

To thoroughly describe how the *Arabidopsis* proteome was altered by the absence of ATG8 and to relate the resulting phenotypic changes to specific cellular dysfunctions, we compared the global protein profiles of *atg8-9m*, *atg5-1*, and *atg7-2* seedlings to that of WT by shotgun LC-MS/MS. Here, 7-d-old seedlings grown under normal conditions, as well as under nitrogen- or fixed-carbon starvation conditions, were digested with trypsin, and their total proteomes were then analyzed in bulk by label-free quantification using the precursor ion intensities obtained from the MS1 scans as a semi-quantitative measure of protein abundance (McLoughlin *et al.*, 2018). Each genetic background/treatment was analyzed by four biological replicates, each of which was assessed by two technical replicates. To be included in the analyses, each protein had to be detected by at least one peptide in each of the four biological replicates from at least one genotype when comparing the *atg8-9m* mutant to the WT or the *atg5-1* or *atg7-2* mutants. When comparing *atg8-9m* vs WT, our MS/MS data quantified a total of 5928 and 4322 individual proteins in nitrogen- and fixed-carbon-starved samples, respectively (Tables S2–S4).

Consistent with previous *Arabidopsis* and maize proteomic studies (Avin-Wittenberg *et al.*, 2015; McLoughlin *et al.*, 2018; Havé *et al.*, 2019), principal component analysis (PCA) showed that both genotype and nutrient starvation profoundly affected the *Arabidopsis* proteome profiles. Here, the proteome of *atg8-9m* seedlings behaved similarly to those of *atg5-1* and *atg7-2* mutants under both nonstarved and starved conditions (Fig. S7). In fact, all three mutant genotypes clustered with each other by PCA and well away from the WT for both treatments (Fig. S7a), indicating that the proteomes of seedlings missing ATG8 generally respond similarly to those missing ATG5 and ATG7. While ATG8 peptides were easily detected in the *atg5-1* and *atg7-2* samples, they were not detected in the *atg8-9m* samples (Fig. S7d,e), which is consistent with the effects of the mutations and supported by the lack of detectable ATG8 seen by immunoblotting seedling samples (Fig. 1c).

To better define how the *Arabidopsis* proteome was altered by *atg8* mutation and/or nutrient starvation, we generated volcano plots to analyze the behavior of all detected proteins of *atg8-9m* seedlings against WT, as compared to *atg5-1* and *atg7-2* plants. As shown in Figs 3(a), S7(c), and S8, whereas the total detected proteins in the plots were evenly distributed between the WT

© 2025 The Author(s).
New Phytologist © 2025 New Phytologist Foundation.

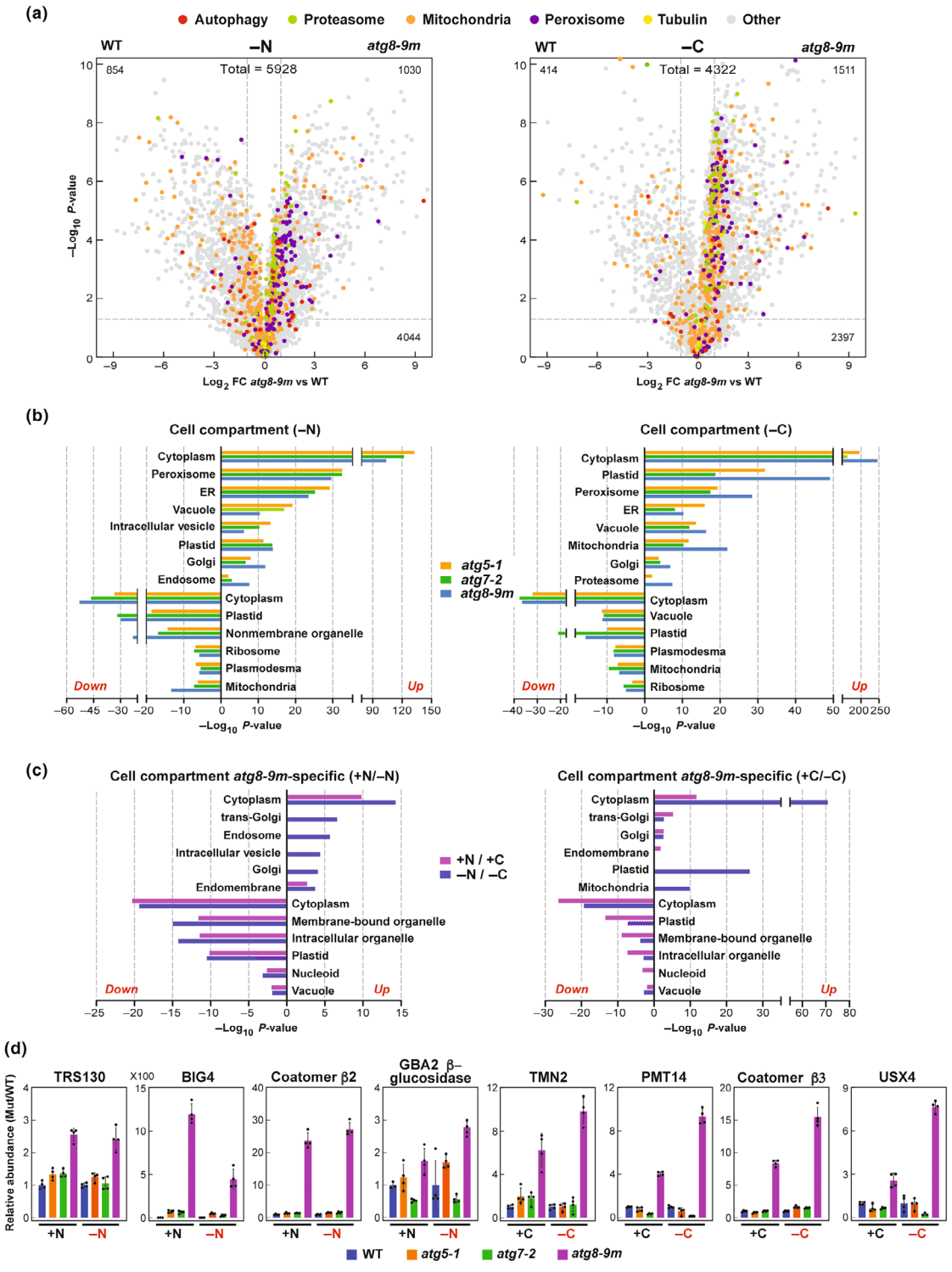

Fig. 3 *Arabidopsis* proteome is strongly affected by the *atg8-9m* mutation. (a) Volcano plots showing the preferential accumulation of proteins categorized by Gene Ontology (GO) to autophagy process, 26S proteasome complex, and specific cellular compartments in *atg8-9m* vs wild-type (WT) seedlings under N or C starvation. Protein abundances were measured using MS1 precursor ion intensities based on the average of three biological replicates, each analyzed in quadruplicate. Proteins assigned to the autophagy, proteasome, mitochondria, and peroxisome are colored in red, green, orange, and purple, respectively. Detected tubulins and proteins within other GO categories are labeled in yellow and gray, respectively. (b) Log_{10} fold enrichment/depletion using a singular enrichment of specific GO terms for proteins that were consistently altered in abundance in the *atg* mutants compared with that in the WT (–N or –C). (c) Specific GO terms for proteins that were significantly enriched or depleted only in the *atg8-9m* plants. (d) Levels of representative Golgi proteins specifically affected by the *atg8-9m* mutant. Each value was normalized to the average value of the WT and presented as mean ± SD (n = 3 biological replicates, each analyzed in quadruplicate by MS).

© 2025 The Author(s).
New Phytologist © 2025 New Phytologist Foundation.

14698137, 0, Downloaded from https://nph.onlinelibrary.wiley.com/doi/10.1111/nph.70418 by University Of British Columbia, Wiley Online Library on [01/09/2025]. See the Terms and Conditions (https://onlinelibrary.wiley.com/terms-and-conditions) on Wiley Online Library for rules of use; OA articles are governed by the applicable Creative Commons License

and *atg8-9m* in nonstarved seedlings, the protein distribution was remarkably skewed toward the *atg8-9m* ledger under both nitrogen and fixed-carbon starvation, indicating that the *atg8-9m* mutant stabilized a subset of the total proteome under these stresses. For example, 17.3% (1030) and 34.9% (1511) of the detected proteins were significantly more abundant in nitrogen- and fixed-carbon-starved *atg8-9m* samples, respectively ($P < 0.05$; FDR < 0.05), whereas only 14.4% (854) and 9.5% (414) were significantly less abundant (Fig. 3a). A similar skew of the proteome profile was also observed in starved *atg5-1* and *atg7-2* samples (Fig. S7d,e). Many of the same proteins showed similar shifts in relative abundance in the *atg8-9m*, *atg5-1*, and *atg7-2* seedlings as compared with those in the WT, consistent with similar impacts of the mutations on autophagy and proteome dysfunction (Fig. S9). A good example was the autophagic receptor NBR1, which was more abundant in all three mutant backgrounds than in the WT after starvation (Figs S7c–e, S8). Preferential enrichments were also seen for proteins associated with the chloroplasts, endoplasmic reticulum (ER), mitochondria, ribosomes, peroxisomes, proteasomes, and peroxisomes in the mutant backgrounds, with the most robust increases seen for ER, mitochondria, peroxisomes, and proteasome proteins during starvation (Fig. S9), which is consistent with prior studies showing that these compartments/complexes are robust targets of starvation-induced autophagy (McLoughlin *et al.*, 2018, 2020; Havé *et al.*, 2019; Barros *et al.*, 2023; Muhammad *et al.*, 2024). Several notable proteins increased substantially in starved *atg8-9m* samples, especially under fixed-carbon conditions, including the 20S proteasome alpha subunit G1 (PAG1), 20S proteasome alpha subunit E1 (PAE1), and 26S proteasome regulatory particle AAA-ATPase 2a (RPT2a) subunits of the proteasome; peroxisome isocitrate lyase (ICL) and peroxisomal biogenesis factor 7 (PEX7) from the peroxisome; MEE4 and TIM13 from mitochondria; and the autophagic cargoes/receptors 26S proteasome non-ATPase regulatory subunit 4 (RPN10), ubiquitin-binding protein DOMINANT SUPPRESSOR of KAR2 (DSK2a), ATG1a, and peroxisome biogenesis protein 6 (PEX6) (Fig. S8).

The global effects of the *atg8-9m* mutations on compartment/complex profiles and their similarity to those seen for the *atg5-1* and *atg7-2* proteomes were further highlighted by GO term enrichment analyses (Fig. 3b). Terms related to the cytoplasm, peroxisome, ER, vacuole, plastid, intracellular vesicle, Golgi, and endosomes were prominent in nitrogen-starved samples from all three mutant backgrounds, with the addition of the mitochondria term for fixed-carbon-starved samples. To further uncover the specific effects of the *atg8* mutations on compartments/processes, we performed a GO enrichment analysis of the proteins whose abundances were altered by the *atg8-9m* mutations but not paralleled by the *atg5-1* or *atg7-2* mutations (14.3% of total proteins analyzed in +/–N samples and 18.7% in +/–C samples). As shown in Fig. 3(c), a number of GO terms became prominent in the *atg8-9m-specific* datasets. Of particular interest were proteins associated with the *trans*-Golgi network and the Golgi apparatus regardless of nutrient stress (Fig. 3d), consistent with the proposed noncanonical role of ATG8 in maintaining Golgi homeostasis (Zhou *et al.*, 2023). Specific examples of interest include RR130, BIG4, coatomer β2, coatomer β3, GRA2 β-glucosidase, TMN2, PMT14, and UXS4, with several showing dramatically increased levels in the *atg8-9m* mutant relative to the *atg5-1* and *atg7-2* mutants (Fig. 3d).

All ATG8 representative isoforms interact with RABG3 proteins via the AIM-LDS interfaces

To further examine the functional redundancy of *Arabidopsis* ATG8s, we then focused on the late stages of autophagy and investigated ATG8-interacting partners involved in the autophagosome–vacuole fusion. Of particular interest was RABG3f, a member of the RAB7 GTPase family, that was recently shown to interact with ATG8 by yeast two-hybrid (Marshall *et al.*, 2019) and co-immunoprecipitation assays (Rodriguez-Furlan *et al.*, 2019). A study on its yeast and metazoan counterparts, Ypt7 and RAB7 respectively, revealed that they are important regulators of multiple endocytic and autophagic processes, including trafficking, maturation, lysosomal biogenesis and maintenance, and fusion (Zhao *et al.*, 2021). Here, we first confirmed that RABG3f specifically interacts with ATG8a *in planta* by LCI assays (Chen *et al.*, 2008), using constructions expressing RABG3f C terminally fused to the N-terminal fragment of the LUC reporter (RABG3f-nLUC) and ATG8a N terminally fused to the C-terminal fragment of the LUC reporter (cLUC-ATG8a). When RABG3f-nLUC, cLUC-ATG8a, and empty nLUC and cLUC control vectors were co-expressed in tobacco leaves via *A. tumefaciens*-mediated transfection, only the combination simultaneously expressing RABG3f-nLUC and cLUC-ATG8a showed a strong interaction as measured by the bioluminescence signal, whereas combinations expressing RABG3f-nLUC or cLUC-ATG8a with control vectors did not (Fig. 4a). This RABG3f/ATG8 interaction was then confirmed by *in vitro* pull-down assays with the tobacco leaf samples transfected with RABG3-nLUC and then pulled down after extraction with beads coated with GST-ATG8a (Fig. 4b).

Additional LCI assays demonstrated that this interaction is conserved between these two protein families, as RABG3f could interact with the representatives from other major ATG8 clades/subclades, ATG8e and ATG8h, and that ATG8a could interact with other members of the RABG3 family, including RABG3b, RABG3d, and RABG3e (Fig. S10). Furthermore, we examined the interactions of ATG8a with RABG3f in its two nucleotide-binding states. When the WT RABG3f, its GTP-bound, CA RABG3f(CA) variant, and its GDP-bound, DN RABG3f(DN) variant were co-expressed together with ATG8a, they all showed strong LUC complementation by the LCI assay (Fig. S11a), suggesting that the interaction between ATG8a and RABG3f is independent of RABG3f activation. The expression of RABG3/RABG3(CA)-nLUC, RABG3(DN)-nLUC, and cLUC-ATG8a fusions was subsequently validated by immunoblotting with anti-LUC antibodies (Fig. S11b), thus ruling out differential expression or stability.

To identify the residues in RABG3f that bind to ATG8a, we searched for possible AIMs using the iLIR database (Kalvari *et al.*, 2014; https://ilir.warwick.ac.uk/index.php), which yielded

© 2025 The Author(s).
New Phytologist © 2025 New Phytologist Foundation.

14698137, 0, Downloaded from https://nph.onlinelibrary.wiley.com/doi/10.1111/nph.70418 by University Of British Columbia, Wiley Online Library on [01/09/2025]. See the Terms and Conditions (https://onlinelibrary.wiley.com/terms-and-conditions) on Wiley Online Library for rules of use; OA articles are governed by the applicable Creative Commons License

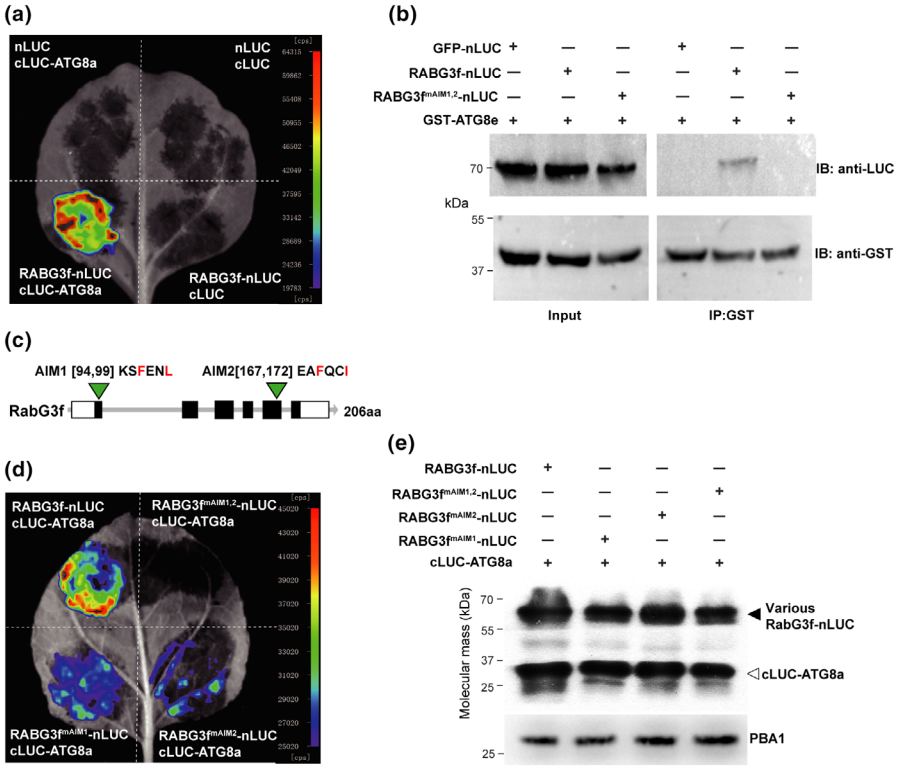

Fig. 4 *Arabidopsis* Rab GTPase (RABG)3f interacts with ATG8 through its ATG8-Interacting Motifs (AIMs). (a) Luciferase (LUC) complementation imaging (LCI) assay to detect the interaction between RABG3f and ATG8a. N-terminal fragment (nLUC) and a C-terminal fragment (cLUC) were used as negative controls. (b) *In vitro* pull-down assay. Protein extracts obtained from tobacco leaves infiltrated with the indicated constructions were incubated with the recombinant GST-ATG8e proteins coupled with glutathione beads to analyze the interaction between ATG8 and RABG3f. Both the input and pull-down samples were subjected to western blotting using anti-LUC or anti-GST. (c) Structure of the *RABG3f* gene including the AIMs and the corresponding mutations in the AIMs. (d) Luciferase complementation between RABG3f and ATG8a was diminished by the AIM mutations in RABG3f. (e) The abundance of cLUC and nLUC fusion proteins in (d) was validated by immunoblotting with anti-LUC antibody, which recognizes both nLUC and cLUC of luciferase. Antibody against PBA1 was used as a loading control.

two candidate AIM sequences that are well-conserved within the RABG3 GTPase family, namely AIM1 (KSFENL, Residues 94–99 in RABG3f) and AIM2 (EAFQCI, Residues 167–172 in RABG3f), respectively (Fig. S12). To confirm their roles in ATG8 binding, we mutated the key residues to alanine in AIM1 (RABG3f^{mAIM1}: F96A L99A) and AIM2 (RABG3f^{mAIM2}: F169A I172A), then tested full-length RABG3f for its ability to bind to ATG8a using the LCI assay (Fig. 4c). While the mutations in AIM1 or AIM2 individually decreased RABG3f binding to ATG8a, the mutations in both AIMs completely abolished the interaction (Fig. 4d,e), indicating that both AIMs promote ATG8 binding. We discounted the possibility of differential expression levels or protein stability as both RABG3f and its AIM-mutated variants accumulated well *in planta* when transiently expressed by the *35S* promoter in tobacco leaves and observed by immunoblotting (Fig. 4e).

RABG3f localizes to autophagosomal membrane

Given that RABG3f interacts with ATG8s through an AIM-LDS interface, we hypothesized that ATG8 might recruit RABG3f to autophagosomes during fusion with the vacuole. To test this notion, we attempted to colocalize mCherry-RABG3f to GFP-ATG8a by confocal fluorescence microscopy of stable transgenic *Arabidopsis* lines expressing both reporters *in planta*. As shown in Fig. 5, much of the mCherry-RABG3f signal appeared as puncta in N-starved root tip cells, *c.* 66% of which colocalized with GFP-ATG8a (Fig. 5a,d). Remarkably, some of these mCherry-RABG3f-labeled structures appeared as rings (Fig. 5b,c). However, after combining N starvation with ConA treatment, the colocalization dissolved. The ratio of GFP-ATG8a colocalized with mCherry-RABG3f puncta to total GFP-ATG8a puncta dropped significantly to *c.* 4% (Fig. 5d), as most of the GFP-ATG8 signal localized to vacuole-deposited autophagic bodies, while the mCherry-RABG3f signal remained in the cytoplasm.

To better visualize the localization of RABG3f relative to autophagosomes, we introduced the mCherry-RABG3f and mCherry-ATG8a reporters into the *gfs9-4* mutant. A previous study has shown that GFS9 is a peripheral protein of the Golgi apparatus whose deficiency induces membrane trafficking defects, including the abnormal accumulation of dilated late endosomes and autophagosome-like structures (Ichino *et al.*, 2014). When GFP-ATG8a was introduced alone into the *gfs9-4* mutant, confocal fluorescence microscopy revealed enlarged GFP-ATG8a dots that aggregated around the perivacuolar regions of root cells after nitrogen starvation and ConA treatment. These dots contrasted with the smaller, vacuolar-resident dots found in the WT (Fig. S13). Under similar conditions, GFP-ATG8a- and mCherry-RABG3-positive structures were observed in the *gfs9-4* mutant; here, the mCherry-RABG3f signals appeared as rings surrounding the ATG8a-positive dots, suggesting that the RABG3f protein associates with autophagosome membranes (Fig. 5e).

Loss of RABG3 GTPases confers hypersensitivity to nutrient stress

To help define the roles of RABG3 proteins during autophagy, we then phenotypically analyzed the sextuple mutant *rabg3a,b,c,d,e,f*, which lacks all six RABG3 isoforms (abbreviated as *rabg3-*

© 2025 The Author(s).
New Phytologist © 2025 New Phytologist Foundation.

14698137, 0, Downloaded from https://nph.onlinelibrary.wiley.com/doi/10.1111/nph.70418 by University Of British Columbia, Wiley Online Library on [01/09/2025]. See the Terms and Conditions (https://onlinelibrary.wiley.com/terms-and-conditions) on Wiley Online Library for rules of use; OA articles are governed by the applicable Creative Commons License

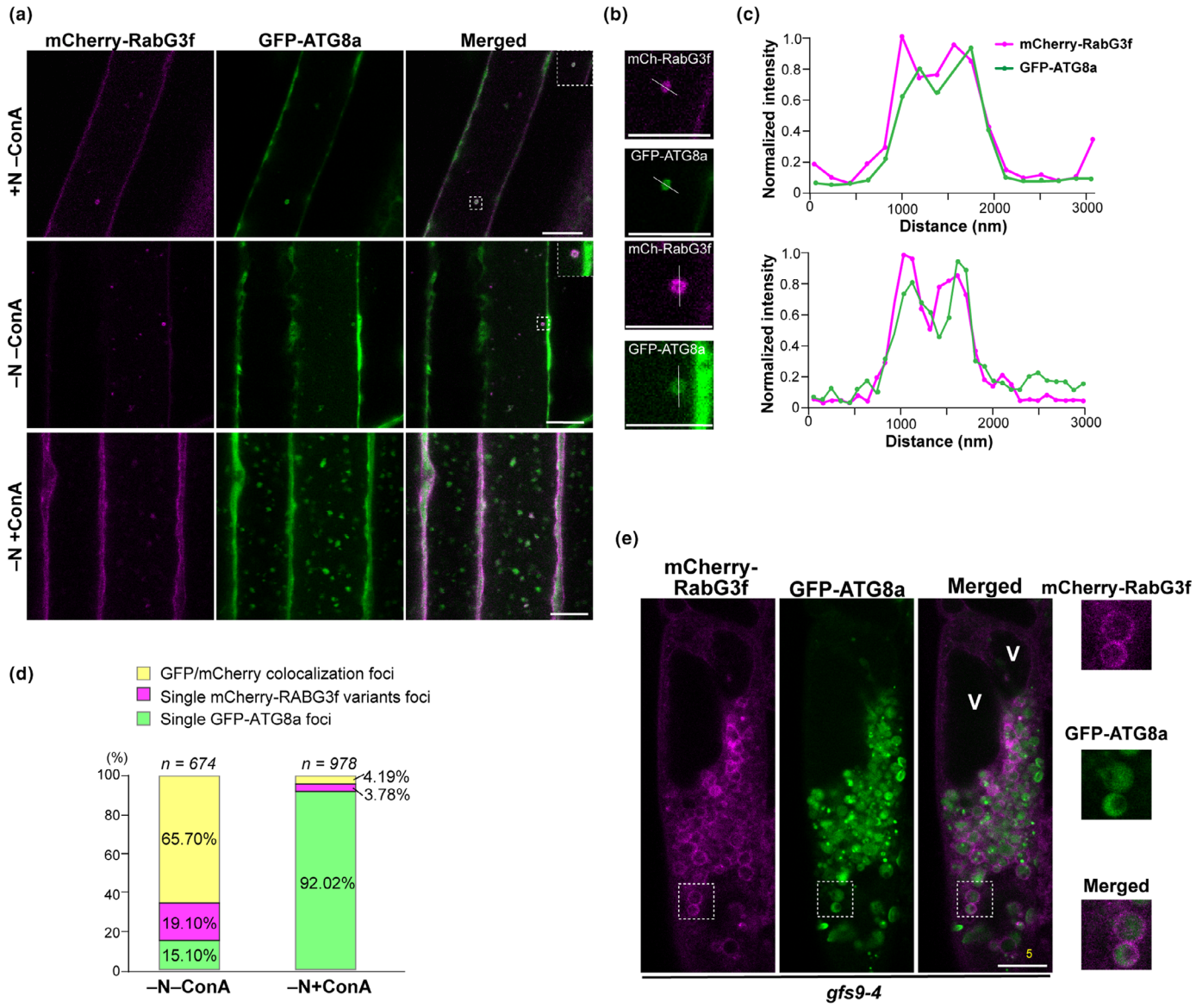

Fig. 5 *Arabidopsis* Rab GTPase (RABG)3f associates with autophagic vesicles. (a) mCherry-RABG3f colocalizes with green fluorecent protein (GFP)-ATG8a in autophagic vesicles. Wild-type (WT) plants stably expressing both reporters were grown on Murashige and Skoog (MS) medium for 6 d and then transferred to nitrogen-deficient medium plus 1 μM concanamycin A (–N + ConA) or dimethyl sulfoxide (DMSO) (–N–ConA) for 8 h before confocal microscopy. Insets show 3x magnifications of the dashed boxes. Bars, 10 μm. (b, c) Enlarged split-channel images corresponding to the dashed boxes in (a). Intensity profiles along the indicated white lines are plotted in (c). Bars, 5 μm. (d) Quantification of the colocalization ratio between RABG3f and autophagosomal marker ATG8. A total of $n = 674$ (–N–ConA) and $n = 978$ (–N + ConA) particles were used for colocalization ratio calculations. (e) mCherry-RABG3f forms ring-like structures and colocalizes with GFP-ATG8a in the *gfs9-4* mutant. Mutant seedlings stably expressing both reporters were grown on MS medium for 6 d and then exposed to nitrogen-deficient medium containing 1 μM ConA for 8 h before confocal microscopy. The far-right panels show the magnifications of the white dashed boxes. V, vacuole. Bars, 5 μm.

6m) (Ebine *et al.*, 2014), and compared it with the *atg7-2* and *atg8-9m* mutants. When grown in nutrient-rich soil, *rabg3-6m* plants senesced earlier than the WT but slightly later than the *atg7-2* and *atg8-9m* controls grown under a LD photoperiod (Fig. 6a). Such early senescence phenotypes became more pronounced when grown under SD conditions. Premature leaf yellowing was seen after *c.* 10 wk in the *rabg3-6m*, *atg7-2*, and *atg8-9m* mutants, whereas WT plants remained relatively green and healthy (Fig. S14).

When grown on nitrogen-limited MS medium, the *rabg3-6m* mutant also displayed phenotypically accelerated senescence-like symptoms compared with the WT, and its Chl content declined significantly faster than that of the WT but slower than those of the *atg7-2* and *atg8-9m* mutants. (Fig. 6b,e). Notably, the *rabg3-6m* mutant developed shorter roots than the WT when grown on a nitrogen-depleted medium, resembling the *atg7-2* and *atg8-9m* mutants. Additionally, transient fixed-carbon starvation experiments revealed that the *rabg3-6m* seedlings, such as *atg5-1* and

© 2025 The Author(s).
New Phytologist © 2025 New Phytologist Foundation.

14698137, 0, Downloaded from https://nph.onlinelibrary.wiley.com/doi/10.1111/nph.70418 by University Of British Columbia, Wiley Online Library on [01/09/2025]. See the Terms and Conditions (https://onlinelibrary.wiley.com/terms-and-conditions) on Wiley Online Library for rules of use; OA articles are governed by the applicable Creative Commons License

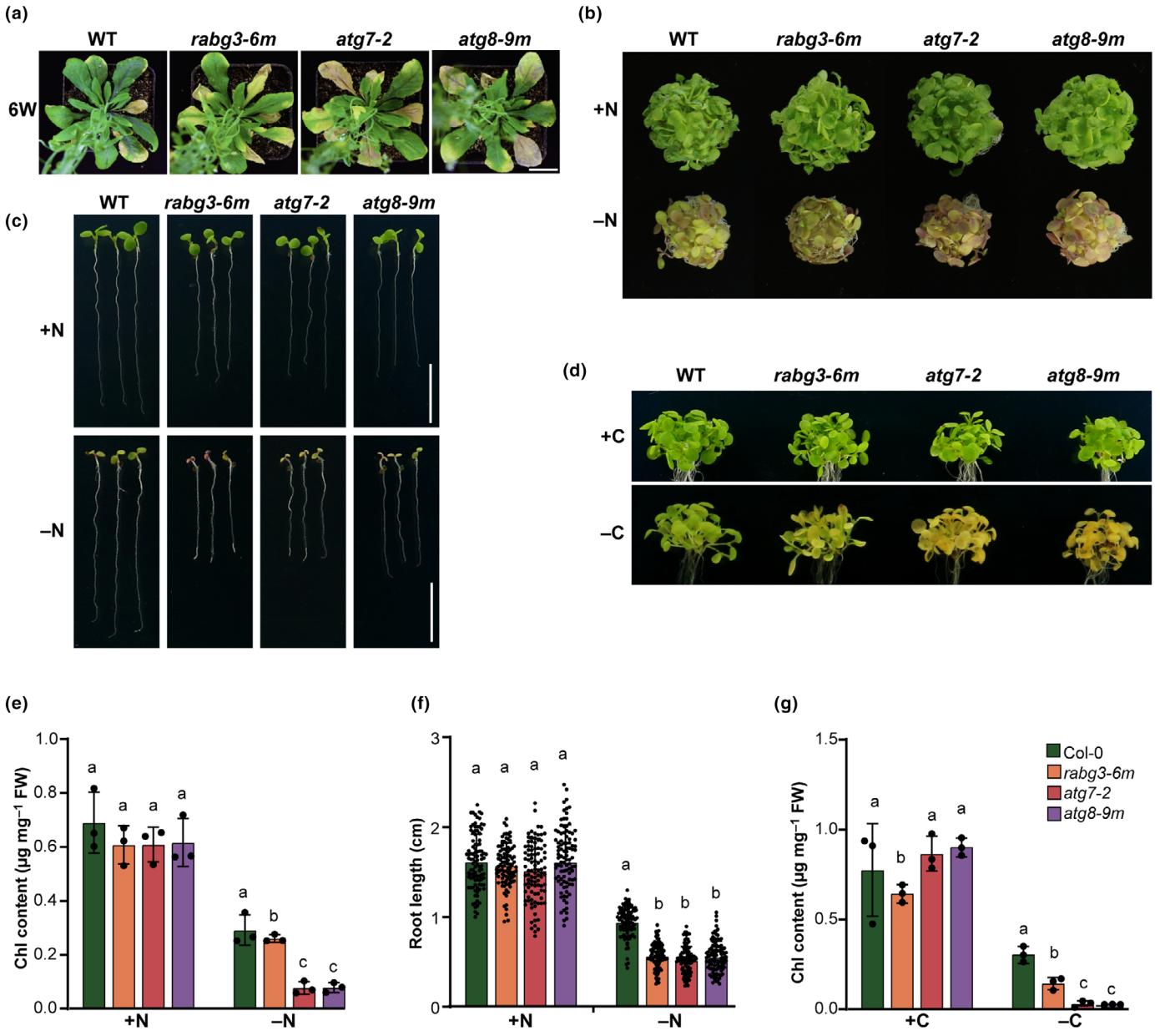

Fig. 6 Phenotypic analyses of the *Arabidopsis rabg3a,b,c,d,e,f* (*rabg3-6m*) sextuple mutant. The homozygous *rabg3-6 m* mutant, the autophagy mutants *atg7-2* and *atg8-9m*, and wild-type (WT) were included for comparison. (a) Accelerated senescence. Plants were grown at 22°C in nutrient-rich soil under long-day (LD) conditions for 6 wk. Bar, 1 cm. (b) Enhanced sensitivity to nitrogen starvation. Seeds were germinated in 1× Murashige and Skoog (MS) liquid medium and grown under constant white light conditions for 1 wk, and then transferred to either fresh MS (+N) or nitrogen-deficient (–N) liquid medium for an additional 1 wk. (c) Short primary root phenotype of *rabg3-6m* in response to nitrogen starvation. Seeds were germinated and grown vertically on MS medium with (+N) or without nitrogen (–N) under LD conditions for 1 wk before imaging and root length quantification. Bars, 5 mm. (d) Senescence phenotypes of the *rabg3-6m* mutant after dark treatment. Seedlings were germinated and grown on ½MS solid medium with 1% sucrose under LD conditions for 1 wk, then transferred to ½MS medium without sucrose (–C) and grown vertically in the dark for another 7 d before imaging. (e) Total Chl content of the plants shown in (b). Data are presented as mean ± SD (n = 3 biological replicates, 80–120 seedlings per genotype in each independent experiment). (f) Quantification of root length of plants shown in (c). Data are presented as mean ± SD (n = 3 biological replicates, 30–40 seedlings per genotype in each independent experiment). (g) Total Chl content of the plants shown in (d). Data are presented as mean ± SD (n = 3 biological replicates, 80–120 seedlings per genotype in each independent experiment). Different letters in (e, f, g) indicate significant differences ($P < 0.05$) as determined using two-way ANOVA followed by Tukey's multiple comparison test.

atg7-2 seedlings, were hypersensitive to fixed-carbon stress (Jia *et al.*, 2019; Sun *et al.*, 2023). As compared with the WT, all three mutants senesced prematurely when grown on ½MS medium supplemented with Suc under an LD photoperiod for 1 wk, and then transferred to ½MS medium without added Suc and kept in the dark for 10 d (Fig. 6d,g). Taken together, the loss

© 2025 The Author(s).
New Phytologist © 2025 New Phytologist Foundation.

14698137, 0, Downloaded from https://nph.onlinelibrary.wiley.com/doi/10.1111/nph.70418 by University Of British Columbia, Wiley Online Library on [01/09/2025]. See the Terms and Conditions (https://onlinelibrary.wiley.com/terms-and-conditions) on Wiley Online Library for rules of use; OA articles are governed by the applicable Creative Commons License

of all six RABG3 isoforms resulted in early senescence and increased sensitivity to nutrient stress, similar to that observed in mutants lacking core autophagy components.

Autophagic activity is downregulated in *rabg3-6m* mutant

Given that RABG3f might be involved in autophagy, we investigated this possibility by examining the behavior of GFP-ATG8a when it was transiently expressed in the leaf protoplasts prepared from WT and *rabg3-6 m* plants (Fig. 7a). Notably, upon ConA treatment, GFP-ATG8a-labeled puncta localized to vacuoles were substantially fewer in *rabg3-6m* cells (*c.* 3.5-fold less) than in the WT (Fig. 7b). Next, we examined the localization of GFP-ATG8a relative to the lytic vacuole marker Aleu-GFP. This marker was created by a fusion of GFP to the vacuolar sorting signal of the barley (*Hordeum vulgare*) protease Aleurain (Di Sansebastiano *et al.*, 2001), which, when expressed *in planta*, is trafficked to the central vacuole via the ER, Golgi, and PVC route. When Aleu-GFP was transiently expressed in protoplasts, most WT cells displayed a diffuse vacuolar fluorescence. By contrast, bright punctate structures were detected in *rabg3-6m* cells in addition to the faint diffuse vacuolar fluorescence (Fig. S15a). These punctate structures might represent Aleu-GFP abnormally accumulating in early endocytic compartments when its vacuolar trafficking is blocked, which has been observed in several *Arabidopsis* endocytic mutants (Sanmartin *et al.*, 2007; Zeng *et al.*, 2015; Kim *et al.*, 2022). The block of Aleu-GFP transport in the *rabg3-6m* mutant was further validated using a GFP release immunoblot assay. As shown in Fig. S15(b), while GFP was almost completely released in WT cells 8 h after transfection, indicating endocytic transport of the marker to the vacuole, a substantial amount of the intact Aleu-GFP fusion was still evident in *rabg3-6m* cells, indicating a block in endocytosis. Unlike the autophagic marker GFP-ATG8a and the vacuolar marker Aleu-GFP, the vacuolar trafficking of ABS3-GFP was unaffected in *rabg3-6 m* protoplasts, suggesting that the ABS3-ATG8 proteolysis pathway does not require the RABG3 GTPase (Fig. S15c,d).

To further confirm this notion, we stably introduced by conventional *A. tumefaciens*-mediated transformation GFP-ATG8a into the *rabg3-6m* background to monitor the autophagic flux. After combined nitrogen starvation and ConA treatment, GFP-ATG8a puncta were readily detected in WT root cells, whereas in *rabg3-6m*, vacuolar deposition of GFP-ATG8a puncta was inhibited; here, *c.* 2.5-fold fewer GFP-ATG8a puncta accumulated in *rabg3-6m* roots than in WT roots (Fig. 7c,d). Autophagic flux was suppressed as well, as evidenced by the decreased ratio of free GFP to GFP-ATG8a fusion in the *rabg3-6m* mutant compared with that in the WT in response to nitrogen starvation (Fig. 7e). We also measured the levels of several ATG proteins by immunoblotting of total seedling extracts to determine how RABG3 affects the autophagy system generally. As shown in Fig. 7(f), levels of ATG8 and ATG1a hyperaccumulated in the *rabg3-6m* mutant as compared with that in the WT, consistent with the evidence showing that autophagic defects suppress their turnover (Thompson *et al.*, 2005; Phillips *et al.*, 2008; Chung *et al.*, 2010; Li *et al.*, 2014; Huang *et al.*, 2019). However, the levels of ATG5 and its conjugation to ATG12 remained unaffected in this mutant (Fig. 7f). Collectively, the data support a role for the RABG3 GTPase in plant autophagy.

RABG3-ATG8 interaction is essential for the vacuolar deposition of autophagic vesicles

In light of our discovery of the RABG3-ATG8 interaction and the association of RABG3f with the autophagosome, we ask whether this interaction is essential for the vacuolar deposition of autophagosomes. To test this possibility, we first transiently co-expressed GFP-ATG8a with either mCherry-RABG3f or mCherry-RABG3f^{mAIM1,2} (an AIM mutant) in the protoplasts prepared from *rabg3-6m* leaves. As shown in Fig. 8(a,b), the accumulation of GFP-ATG8a puncta in the vacuole was readily observed in the *rabg3-6m* cells expressing mCherry-RABG3f after ConA treatment, whereas much fewer GFP-ATG8a puncta (*c.* 12-fold fewer) were detected in similarly treated protoplasts expressing the mCherry-RABG3f^{mAIM1,2} variant, indicating that the expression of mCherry-RABG3f, but not of mCherry-RABG3f^{mAIM1,2}, can complement the *rabg3-6 m* defect that compromises the vacuolar deposition of autophagosomes.

The importance of the AIM motifs of RABG3f for the vacuolar trafficking of ATG8 was further confirmed by a GFP-ATG8 cleavage assay as shown in Fig. 8(c). Conversely, when the vacuolar marker Aleu-GFP was co-expressed with either the mCherry-RABG3f or mCherry-RABG3f^{mAIM1,2} variant, most *rabg3-6m* protoplasts showed a strong diffuse green vacuolar fluorescence regardless of which RABG3f version was expressed (Fig. 8d). Moreover, the block of Aleu-GFP fusion processing in the *rabg3-6 m* mutant could be reversed by expressing either mCherry-RABG3f or mCherry-RABG3f^{mAIM1,2} (Fig. 8e), suggesting that the endocytic trafficking of Aleu-GFP is independent of the RABG3f-ATG8 interaction.

To further investigate whether the RABG3-ATG8 interaction is essential for the autophagic pathway in *Arabidopsis*, and to confirm the *rabg3-6 m* phenotypes by complementation, we tested two RABG3f vectors expressed under the control of the *Arabidopsis UBQ10* promoter in plants expressing GFP-ATG8a: One was WT RABG3f while the other was complemented with the AIM-mutated RABG3f^{mAIM1,2} variant (Fig. S16a). Immunoblot analysis of representative transgenic plants showed that both RABG3f reporters and GFP-ATG8a were co-expressed (Fig. S16b). Phenotype analyses revealed that the line complemented with the WT RABG3f grew similarly to WT under all tested conditions, including senescence, nitrogen-limiting, and carbon-limiting conditions. By contrast, the line complemented with the AIM-mutated RABG3f^{mAIM1,2} variant still behaved similarly to the *rabg3-6 m* mutant (Fig. 9a–g). Interestingly, this reporter successfully rescued the trafficking and processing defects of 12S globulin precursor in the *rabg3-6m* mutant (Fig. S16c), which is consistent with the trafficking and processing observations for Aleu-GFP, and further suggests that this RABG3f

© 2025 The Author(s).
New Phytologist © 2025 New Phytologist Foundation.

14698137, 0, Downloaded from https://nph.onlinelibrary.wiley.com/doi/10.1111/nph.70418 by University Of British Columbia, Wiley Online Library on [01/09/2025]. See the Terms and Conditions (https://onlinelibrary.wiley.com/terms-and-conditions) on Wiley Online Library for rules of use; OA articles are governed by the applicable Creative Commons License

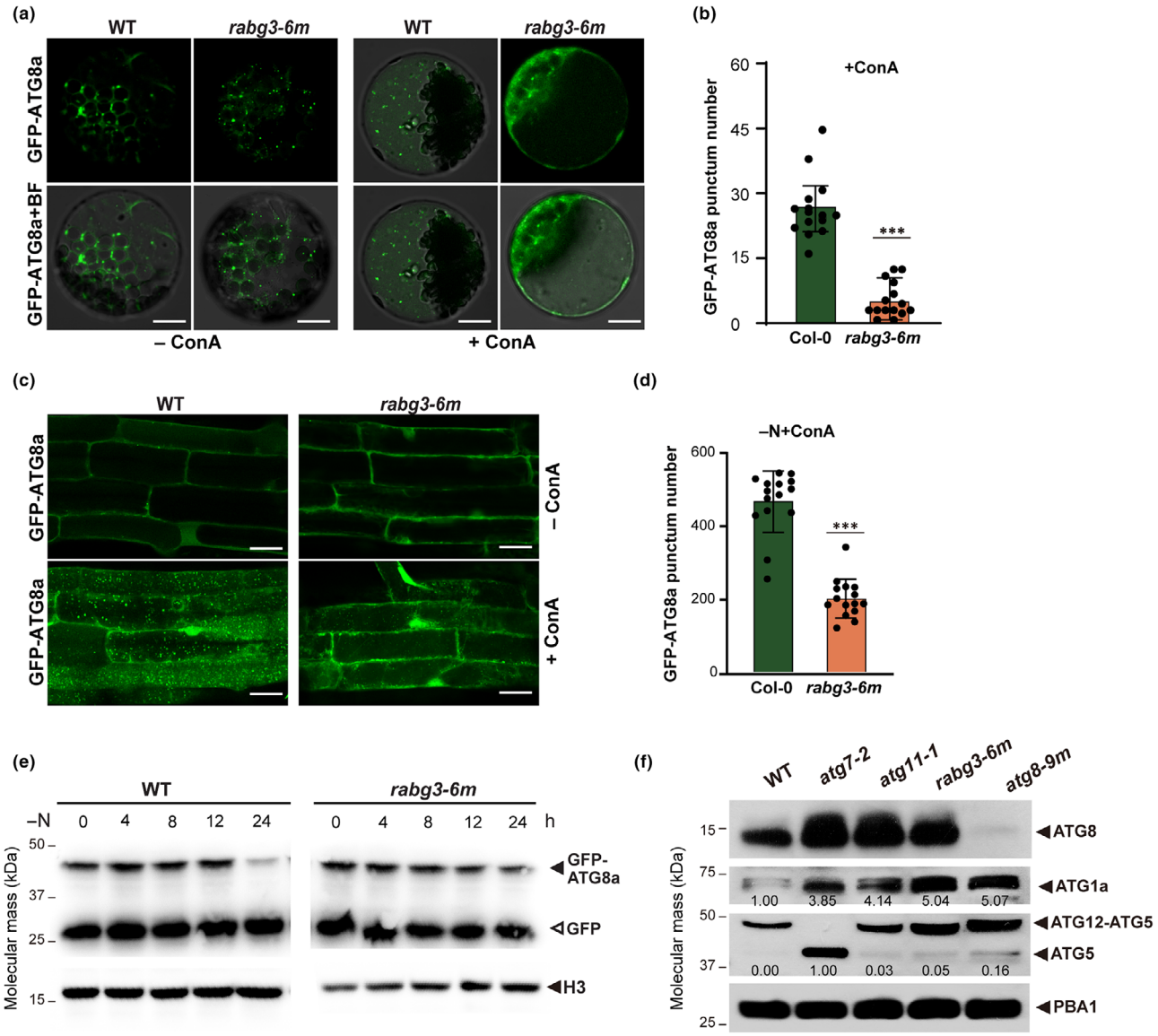

Fig. 7 Lack of Rab GTPase (RABG)3 blocks the deposition of autophagic body in the vacuole. (a, b) Effects of *rabg3* mutations on the vacuolar transport of green fluorecent protein (GFP)-ATG8a in leaf protoplasts. Leaf protoplasts of *Arabidopsis* wild-type (WT) and *rabg3-6m* mutant were transformed with the GFP-ATG8a constructions and treated with 1 μM concanamycin (ConA) for 12 to 14 h before confocal imaging analysis. Bars, 10 μm. Quantification of GFP-ATG8a puncta shown in (b). Images (n = 15) were collected to measure the number of puncta. Data are presented as mean ± SD and asterisked columns represent *rabg3-6m* mutants that are significantly different from WT, according to Student's t-test. ***, $P < 0.001$. Bars, 10 μm. (c, d) Effects of *rabg3* mutations on the vacuolar deposition of GFP-ATG8a in stably transgenic plants. Seedlings expressing GFP-ATG8a were grown on nitrogen-containing Murashige and Skoog (MS) solid medium for 6 d and then transferred to nitrogen-deficient medium supplemented with 1 μM ConA (–N + ConA) or dimethyl sulfoxide (DMSO) (–N–ConA) for another 8 h before confocal fluorescence microscopy analysis of root cells. Quantification of GFP-ATG8a puncta shown in (d). Images (n = 15) were collected to measure the number of puncta. Data are presented as mean ± SD and asterisked columns represent *rabg3-6m* mutants that are significantly different from WT, according to Student's t-test. ***, $P < 0.001$. Bars, 10 μm. (e) Immunoblot detection of the free GFP released during the vacuolar degradation of GFP-ATG8a. One-week-old WT and *rabg3-6m* seedlings described in (c) were transferred to fresh liquid MS medium without nitrogen (–N) for the indicated time. Total protein was subjected to immunoblot analysis using anti-GFP antibodies. The GFP-ATG8a fusion and free GFP are indicated by closed and open arrowheads, respectively. H3 was used to confirm approximately equal protein loading. (f) Immunoblot detection of multiple ATG proteins from WT, *rabg3-6m*, *atg7-2*, *atg11-1*, and *atg8-9m* mutants using antibodies against ATG8, the autophagy-related 1a, a serine/threonine-protein kinase (ATG1a), and ATG5, respectively. Antibody against PBA1 was used as a loading control. Numbers below bands indicate the ATG1a/PBA1 or free ATG5/PBA1 ratios in the labeled lanes. For ATG1a/PBA1 ratios, the WT ratio is normalized to 1.0. For free ATG5/PBA1 ratios, the ratios of WT and *atg7-2* are normalized to 0.0 and 1.0, respectively.

variant can still participate in the endocytic function of *Arabidopsis* RAB7/RABG3s, but not in its autophagic functions. We further investigated whether there was a difference in the autophagy pathway between the complementation lines. As shown in Fig. 9(h–j), confocal imaging analysis and quantification revealed that, under nitrogen-limiting conditions, most of

© 2025 The Author(s).
New Phytologist © 2025 New Phytologist Foundation.

14698137, 0, Downloaded from https://nph.onlinelibrary.wiley.com/doi/10.1111/nph.70418 by University Of British Columbia, Wiley Online Library on [01/09/2025]. See the Terms and Conditions (https://onlinelibrary.wiley.com/terms-and-conditions) on Wiley Online Library for rules of use; OA articles are governed by the applicable Creative Commons License

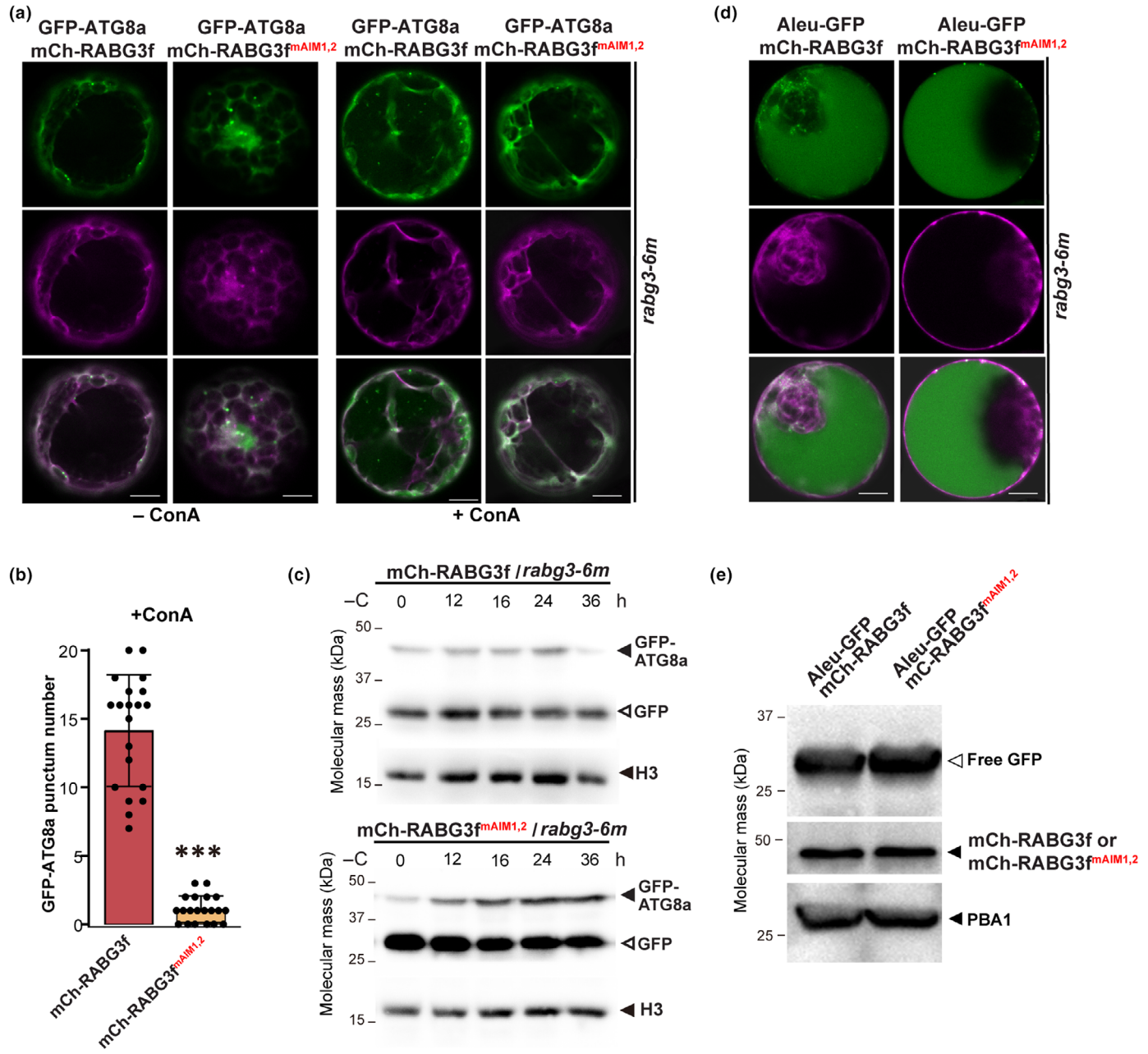

Fig. 8 *Arabidopsis* Rab GTPase (RABG)3f mediates the vacuolar deposition of green fluorecent protein (GFP)-ATG8a via its ATG8-interacting motif (AIMs). (a, b) Confocal images of protoplasts prepared from *rabg3-6m* transiently coexpressing GFP-ATG8a with either mCherry-RABG3f or mCherry-RABG3f^{mAIM1,2}. Leaf protoplasts were incubated in liquid medium containing dimethyl sulfoxide (DMSO) (–ConA) or concanamycin A (+ConA) for 12 h before observation. Bars, 10 μm. Quantification of vacuolar puncta of ABNORMAL SHOOT3 (ABS3)-GFP shown in (b). Images (n = 20) were collected to measure the number of puncta. Data are presented as mean ± SD and asterisked columns represent protoplasts expressing the mCherry-RABG3f^{mAIM1,2} construction that are significantly different from those expressing the wild-type (WT) form RABG3f, according to Student's t-test. ***, $P < 0.001$. (c) Immunoblot analysis of *rabg3-6m* protoplasts transiently expressing GFP-ATG8a with either mCherry-RABG3f or mCherry-RABG3f^{mAIM1,2} as shown in (a) using anti-GFP antibodies. The GFP-ATG8a fusion and free GFP are indicated by closed and open arrowheads, respectively. H3 was used to confirm approximately equal protein loading. (d) Confocal images of *rabg3-6m* protoplasts transiently expressing Aleu-GFP with either mCherry-RABG3f or mCherry-RABG3f^{mAIM1,2}. Leaf protoplasts were incubated in liquid medium for 8 h before observation. Bars, 10 μm. (e) Immunoblot analysis of *rabg3-6 m* protoplasts transiently expressing Aleu-GFP with either mCherry-RABG3f or mCherry-RABG3f^{mAIM1,2} as shown in (d) using anti-GFP and anti-mCherry antibodies. PBA1 was used to confirm approximately equal protein loading.

the mCherry-RABG3f reporter (74%) colocalized with the GFP-ATG8a reporter, whereas only 6% of the colocalized foci with both reporters were found in the RABG3f^{mAIM1,2} complementation line, further confirming the importance of the RABG3-ATG8 binding and the association of RABG3 with autophagic vesicles.

© 2025 The Author(s).
New Phytologist © 2025 New Phytologist Foundation.

14698137, 0, Downloaded from https://nph.onlinelibrary.wiley.com/doi/10.1111/nph.70418 by University Of British Columbia, Wiley Online Library on [01/09/2025]. See the Terms and Conditions (https://onlinelibrary.wiley.com/terms-and-conditions) on Wiley Online Library for rules of use; OA articles are governed by the applicable Creative Commons License

New Phytologist

Discussion

Defining the full roles of ATG8s in plant autophagy has been difficult due to the genetic redundancy among the large number of *ATG8* genes in plants. To date, most of the knowledge about plant ATG8s has come from studies using mutants defective in ATG8 lipidation or plants overexpressing specific isoforms. Here, we overcame this hurdle in *Arabidopsis* by systematically

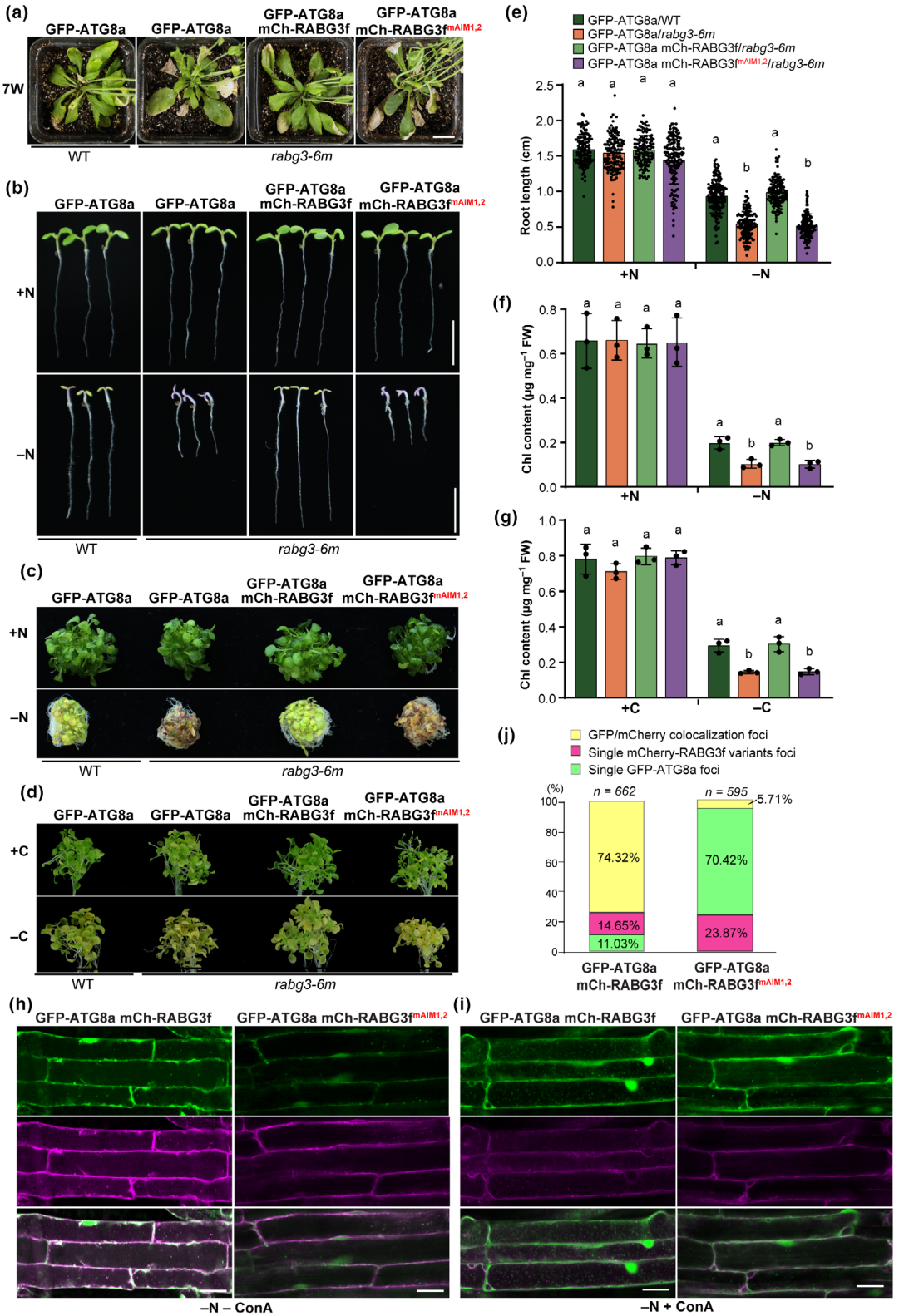

© 2025 The Author(s).
New Phytologist © 2025 New Phytologist Foundation.

14698137, 0, Downloaded from https://nph.onlinelibrary.wiley.com/doi/10.1111/nph.70418 by University Of British Columbia, Wiley Online Library on [01/09/2025]. See the Terms and Conditions (https://onlinelibrary.wiley.com/terms-and-conditions) on Wiley Online Library for rules of use; OA articles are governed by the applicable Creative Commons License

14698137, 0, Downloaded from https://nph.onlinelibrary.wiley.com/doi/10.1111/nph.70418 by University Of British Columbia, Wiley Online Library on [01/09/2025]. See the Terms and Conditions (https://onlinelibrary.wiley.com/terms-and-conditions) on Wiley Online Library for rules of use; OA articles are governed by the applicable Creative Commons License

Fig. 9 Complementation analysis of *Arabidopsis* wild-type (WT) and ATG8-interacting motif (AIM)-mutated Rab GTPase (RABG)3f. (a–g) Wild-type (WT) but not AIM-mutated RABG3f rescues the early senescence and nutrient hypersensitivity of *rabg3-6m*. (a) Senescence assay. Plants were grown on soil at 22°C under a long-day (LD) conditions for 7 wk. Bar, 1 cm. (b) Primary root phenotypes under nitrogen-depleted conditions. Seeds were germinated and grown vertically on Murashige and Skoog (MS) medium with (+N) or without nitrogen (–N) under LD conditions for 1 wk. Bars, 1 cm. (c) Enhanced sensitivity to nitrogen starvation. Seeds were germinated in 1× MS liquid medium and grown under constant white light conditions for 1 wk, and then transferred to either fresh MS (+N) or nitrogen-deficient (–N) liquid medium for an additional 1 wk. (d) Senescence phenotypes after dark treatment. Seedlings were germinated and grown on ½MS solid medium with 1% sucrose under LD conditions for 1 wk, then transferred to ½MS medium without sucrose (–C) and grown vertically in the dark for another 7 d. (e) Quantification of root length of the plants shown in (b). Data are presented as mean ± SD (n = 3 biological replicates, > 50 seedlings per genotype in each independent experiment). (f–g) Total Chl content of the plants shown in (c, d), respectively. Data are presented as mean ± SD (n = 3 biological replicates, 80–120 seedlings per genotype in each independent experiment). Different letters in (e, f, g) indicate significant differences ($P < 0.05$) as determined using two-way ANOVA followed by Tukey's multiple comparison test. (h–j) Confocal fluorescence images of *rabg3-6m* root cells coexpressing green fluorecent protein (GFP)-ATG8a with either mCherry-RABG3f or mCherry-RABG3f^{mAIM1,2}. Six-day-old seedlings were transferred to nitrogen-deficient medium supplemented with or without 1 μM concanamycin A for another 12 h before confocal microscopic observation. Quantification of GFP-ATG8a puncta is shown in (j). Images (n = 15) were collected to measure the number of puncta. Bars, 10 μm.

eliminating the entire *ATG8* family through CRISPR/Cas9-mediated mutagenesis (Figs 1, S1). Phenotypic analyses of various *atg8* mutant combinations, as well as analyses of protein–protein interactions between the ATG8 and RABG3 families, suggest that *Arabidopsis* ATG8s function redundantly in bulky autophagy. This differs from the situation in mammals, in which ATG8 members play distinct roles in the process of autophagosome biogenesis (Weidberg *et al.*, 2010). The double, triple, quadruple, and quintuple mutants did not exhibit obvious differences from the WT roots or shoots either during growth under normal or all nutrient-starved conditions tested, or during senescence. They displayed normal rosette development, flowering times, pollen development, and fecundity (Figs 2, S5, S6). However, we acknowledge that we examined only a few growth conditions, tissue types, and cells, leaving open the possibility that highly specific functions/activities for individual ATG8 isoforms remain to be uncovered with more in-depth phenotypic analyses.

Notably, we discovered that *atg8-9m* are more sensitive to fixed-carbon starvation than those mutants that abolish ATG8/12 conjugation (e.g. *atg7-2* and *atg5-1*), suggesting that ATG8 plays additional roles in carbon starvation-induced senescence which do not involve ATG8 lipidation. A recent study reported that the ABS3 subfamily of MATE proteins promotes carbon starvation-induced senescence through an ATG8-ABS3 interaction and subsequent deposition of ABS3 in the vacuole via a route that does not require the ATG8 conjugation machinery (Jia *et al.*, 2019). However, it remains unclear whether the hypersensitivity to carbon starvation in *atg8-9m* is due to disrupted trafficking of ABS3. In the future, it will be of interest to investigate the molecular mechanism of the noncanonical ATG8-ABS3 interaction that regulates carbon starvation-induced senescence.

Structurally, all ATG8s have ubiquitin-like cores with an N-terminal extension that forms two deep hydrophobic pockets for docking the AIMs of various cargoes/receptors (Johansen & Lamark, 2020). Thus, the structural differences in the hydrophobic pockets and the N termini of ATG8s determine their binding specificity for interacting proteins during selective autophagy. Similar to the metazoan ATG8s, recent studies have begun to reveal the functional specialization of plant ATG8s. Interactome studies and domain swap analysis have shown that a single amino acid polymorphism at the N-terminal β-strand of potato ATG8CL confers binding specificity to a pathogen effector protein (Zess *et al.*, 2019). CLC2, a light chain subunit of the *Arabidopsis* clathrin complex, has been reported to interact specifically with Clade II ATG8 isoforms and to mediate plant immunity against the fungal pathogen *G. cichoracearum* (Lan *et al.*, 2024). The specificity of Clade II ATG8 isoforms was also demonstrated through the overexpression of ATG8I in the *atg4a/b* mutant, which is sufficient to restore the normal rate of autophagosome formation, although it produces smaller autophagosomes (Zou *et al.*, 2025). Using NBR1 as a representative autophagic receptor, we showed that its trafficking was only impaired in *atg8-7 m* and *atg8-9m* protoplasts, but not in other *atg8* mutants (Fig. 1d,f). This probably reflects the broad binding specificity of NBR1 AIMs, as reported previously (Svenning *et al.*, 2011). Nevertheless, the series of *Arabidopsis* mutants generated here lacking different combinations of ATG8s, generated in this study, now allows for the study of their functional specialization.

One possible specialization was through interactions during the autophagosome–lysosome/vacuole fusion possibly through the critical regulator RAB7. It is, therefore, interesting to ask how RAB7 and/or its Rab-specific guanine nucleotide exchange factor (GEF), the MON1-CCZ1 complex, are recruited to the autophagosomal membrane. A yeast study showed that the MON1-CCZ1 complex is targeted to the autophagosome through the interaction between CCZ1 and Atg8 and subsequently promotes RAB7/Ypt7 recruitment (Gao *et al.*, 2018). Another study of fruit fly (*Drosophila melanogaster*) adipocytes proposed that phosphatidylinositol 3-phosphate, produced by the ATG14-containing PI3K complex, is required for the autophagosomal association between the MON1-CCZ1 complex and RAB7 (Hegedűs *et al.*, 2016). Similar findings were observed in tobacco, in which ATG14, paired with ultraviolet resistance-associated gene (UVRAG), another subunit of the class III PI3K complexes, was found to regulate autophagosome maturation by recruiting RAB7 and homotypic fusion and protein sorting complex (HOPS) (Wang *et al.*, 2022). Recently, Zhang *et al.* (2024) reported that the rice MON1-CCZ1 complex is involved in autophagy, most likely through the direct interaction of ATG8 with MON1 rather than with CCZ1. Likewise, rice RAB7 was also found to interact directly with ATG8.

Here, we identified *Arabidopsis* RABG3f as an interacting partner of ATG8 via the AIM-LDS interfaces, which is critical for

© 2025 The Author(s).
New Phytologist © 2025 New Phytologist Foundation.

targeting RABG3f to the autophagosome membrane and likely for the autophagosome–vacuole fusion. Interestingly, we found that this interaction is highly conserved between the RABG3 and ATG8 families (Fig. S10), implying the possible functional redundancy of *Arabidopsis* ATG8 isoforms in the late autophagy stages. Moreover, we discovered that the interaction of RABG3f with ATG8 is independent of its GTP-binding state in the LCI assay (Fig. S11), although this may not represent its physiologically natural state, as both RABG3f and ATG8 were transiently overexpressed. Of course, we cannot exclude the possibility that other factors, such as the MON1-CCZ1 complex and/or UVRAG, are required for the recruitment and/or activation of RAB7 to autophagosomes. Nevertheless, the precise mechanisms by which RAB7 is recruited and activated during plant autophagy remain an area of active investigation.

In conclusion, we have succeeded in generating a nonuple mutant line (*atg8-9m*) eliminating all nine isoforms of ATG8 in *Arabidopsis* by combining mutations that disrupt the Clades I and II ATG8s. By using the mutants that lack different ATG8s, we demonstrated that the two ATG8 clades redundantly control the autophagy activity in *Arabidopsis*. In addition, we discovered that the GTPase RABG3f interacts with ATG8, enabling its association with autophagosome membranes. Further investigations of how ATG8, the MON1-CCZ1 complex, and other factors such as UVRAG and ATG14 act in concert to regulate the recruitment and activation of RAB7 to autophagosomes should improve our understanding of the autophagosome–lysosome/vacuole fusion in plants.

Acknowledgements

This work was supported by grants from the National Natural Science Foundation of China (grant 32370352 to FL and grant 32070195 to Xiao Huang), the Natural Science Foundation of Guangdong Province (2024A1515011671) to Xiao Huang, a grant to FL and RDV from the 111 Center (D23018), and grants to RDV from the US National Science Foundation; Plant Genome Research Program (IOS-1840687) and the US National Institutes of Health; and National Institute of General Medical Sciences (R01-GM124452). We thank Drs Hongbo Li, Cao Yang, and Caiji Gao (South China Normal University, China) for their technical support. We thank Dr Liwen Jiang (The Chinese University of Hong Kong) for the mCherry-VAMP711 construction and Dr Xiaodong Xu (Henan University) for the anti-LUC antibodies.

Competing interests

None declared.

Author contributions

FL, Xiao Huang and RDV designed the research. KD, GD and YL performed most of the experiments. K-EC performed the proteomic analysis. HW, Xiner Huang, WH and PZ provided technical support. TU provided the *rabg-6 m* mutant and technical help to analyze data. FL, Xiao Huang and RDV wrote the manuscript with input from all authors. KD, GD and YL contributed equally to this work.

ORCID

Kuo-En Chen https://orcid.org/0000-0003-0517-9401
Kuntian Dong https://orcid.org/0009-0008-3910-3337
Wanying Huang https://orcid.org/0009-0002-7198-4679
Xiao Huang https://orcid.org/0000-0002-3724-7440
Xiner Huang https://orcid.org/0009-0001-5739-3939
Faqiang Li https://orcid.org/0000-0003-4117-2450
Takashi Ueda https://orcid.org/0000-0002-5190-892X
Richard D. Vierstra https://orcid.org/0000-0003-0210-3516
Huan Wei https://orcid.org/0009-0002-5140-9917
Ping Zheng https://orcid.org/0000-0001-9943-7584

Data availability

All data are available in the main text or in the Supporting Information (Figs S1–S16; Tables S1–S4; Notes S1). The MS proteomics data in this paper have been deposited in the PRoteomics IDEntifications Database (PRIDE; accession no.: PXD059803).

References

Avin-Wittenberg T, Bajdzienko K, Wittenberg G, Alseekh S, Tohge T, Bock R, Giavalisco P, Fernie AR. 2015. Global analysis of the role of autophagy in cellular metabolism and energy homeostasis in *Arabidopsis* seedlings under carbon starvation. *Plant Cell* **27**: 306–322.

Barros JAS, Chatt EC, Augustine RC, McLoughlin F, Li F, Otegui MS, Vierstra RD. 2023. Autophagy during maize endosperm development dampens oxidative stress and promotes mitochondrial clearance. *Plant Physiology* **193**: 1395–1415.

Chen H, Zou Y, Shang Y, Lin H, Wang Y, Cai R, Tang X, Zhou JM. 2008. Firefly luciferase complementation imaging assay for protein–protein interactions in plants. *Plant Physiology* **146**: 323–324.

Chen Q, Soulay F, Saudemont B, Elmayan T, Marmagne A, Masclaux-Daubresse C. 2019. Overexpression of *ATG8* in *Arabidopsis* stimulates autophagic activity and increases nitrogen remobilization efficiency and grain filling. *Plant and Cell Physiology* **60**: 343–352.

Chung T, Phillips AR, Vierstra RD. 2010. ATG8 lipidation and ATG8-mediated autophagy in *Arabidopsis* require ATG12 expressed from the differentially controlled ATG12A and ATG12B loci. *The Plant Journal* **62**: 483–493.

Clough SJ, Bent AF. 1998. Floral dip: a simplified method for Agrobacterium-mediated transformation of *Arabidopsis thaliana*. *The Plant Journal* **16**: 735–743.

Cui Y, Zhao Q, Gao C, Ding Y, Zeng Y, Ueda T, Nakano A, Jiang L. 2014. Activation of the Rab7 GTPase by the MON1-CCZ1 complex is essential for PVC-to-vacuole trafficking and plant growth in *Arabidopsis*. *Plant Cell* **26**: 2080–2097.

Cui Y, Zhao Q, Xie H-T, Wong WS, Wang X, Gao C, Ding Y, Tan Y, Ueda T, Zhang Y *et al.* 2017. MONENSIN SENSITIVITY1 (MON1)/CALCIUM CAFFEINE ZINC SENSITIVITY1 (CCZ1)-mediated Rab7 activation regulates tapetal programmed cell death and pollen development. *Plant Physiology* **173**: 206–218.

Di Sansebastiano GP, Paris N, Marc-Martin S, Neuhaus JM. 2001. Regeneration of a lytic central vacuole and of neutral peripheral vacuoles can be visualized by green fluorescent proteins targeted to either type of vacuoles. *Plant Physiology* **126**: 78–86.

© 2025 The Author(s).
New Phytologist © 2025 New Phytologist Foundation.

14698137, 0, Downloaded from https://nph.onlinelibrary.wiley.com/doi/10.1111/nph.70418 by University Of British Columbia, Wiley Online Library on [01/09/2025]. See the Terms and Conditions (https://onlinelibrary.wiley.com/terms-and-conditions) on Wiley Online Library for rules of use; OA articles are governed by the applicable Creative Commons License

Doelling JH, Walker JM, Friedman EM, Thompson AR, Vierstra RD. 2002. The APG8/12-activating enzyme APG7 is required for proper nutrient recycling and senescence in *Arabidopsis thaliana*. *Journal of Biological Chemistry* **277**: 33105–33114.

Ebine K, Inoue T, Ito J. 2014. Plant vacuolar trafficking occurs through distinctly regulated pathways. *Current Biology* **24**: 375–1382.

Fan T, Yang W, Zeng X, Xu X, Xu Y, Fan X, Luo M, Tian C, Xia K, Zhang M. 2020. A rice autophagy gene *OsATG8b* is involved in nitrogen remobilization and control of grain quality. *Frontiers in Plant Science* **11**: 588.

Gao J, Langemeyer L, Kümmel D, Reggiori F, Ungermann C. 2018. Molecular mechanism to target the endosomal Mon1-Ccz1 GEF complex to the pre-autophagosomal structure. *eLife* **7**: e31145.

Geldner N, Dénervaud-Tendon V, Hyman DL, Mayer U, Stierhof YD, Chory J. 2009. Rapid, combinatorial analysis of membrane compartments in intact plants with a multicolor marker set. *The Plant Journal* **59**: 169–178.

Guerra F, Bucci C. 2016. Multiple roles of the small GTPase Rab7. *Cells* **5**: 34.

Havé M, Luo J, Tellier F, Balliau T, Cueff G, Chardon F, Zivy M, Rajjou L, Cacas JL, Masclaux-Daubresse C. 2019. Proteomic and lipidomic analyses of the *Arabidopsis atg5* autophagy mutant reveal major changes in endoplasmic reticulum and peroxisome metabolisms and in lipid composition. *New Phytologist* **223**: 1461–1477.

Hegedűs K, Takáts S, Boda A, Jipa A, Nagy P, Varga K, Kovács AL, Juhász G. 2016. The Ccz1-Mon1-Rab7 module and Rab5 control distinct steps of autophagy. *Molecular Biology of the Cell* **27**: 3132–3142.

Hu Z, Yang Z, Zhang Y, Zhang A, Lu Q, Fang Y, Lu C. 2022. Autophagy targets Hd1 for vacuolar degradation to regulate rice flowering. *Molecular Plant* **15**: 1137–1156.

Huang X, Zheng C, Liu F, Yang C, Zheng P, Lu X, Tian J, Chung T, Otegui MS, Xiao S *et al.* 2019. Genetic analyses of the *Arabidopsis* ATG1 kinase complex reveal both kinase-dependent and independent autophagic routes during fixed-carbon starvation. *Plant Cell* **31**: 2973–2995.

Ichino T, Fuji K, Ueda H, Takahashi H, Koumoto Y, Takagi J, Tamura K, Sasaki R, Aoki K, Shimada T *et al.* 2014. GFS9/TT9 contributes to intracellular membrane trafficking and flavonoid accumulation in *Arabidopsis thaliana*. *The Plant Journal* **80**: 410–423.

Itakura E, K-I C, Mizushima N. 2012. The hairpin-type tail-anchored SNARE syntaxin 17 targets to autophagosomes for fusion with endosomes/lysosomes. *Cell* **151**: 1256–1269.

Jia M, Liu X, Xue H, Wu Y, Shi L, Wang R, Chen Y, Xu N, Zhao J, Shao J *et al.* 2019. Noncanonical ATG8–ABS3 interaction controls senescence in plants. *Nature Plants* **5**: 212–224.

Johansen T, Lamark T. 2020. Selective autophagy: ATG8 family proteins, LIR motifs and cargo receptors. *Journal of Molecular Biology* **432**: 80–103.

Julian J, Gao P, Del Chiaro A, Carlos De La Concepcion J, Armengot L, Somssich M, Duverge H, Clavel M, Grujic N, Kobylinska R *et al.* 2025. ATG8ylation of vacuolar membrane protects plants against cell wall damage. *Nature Plants* **11**: 321–339.

Kalvari I, Tsompanis S, Mulakkal NC, Osgood R, Johansen T, Nezis IP, Promponas VJ. 2014. iLIR: A web resource for prediction of Atg8-family interacting proteins. *Autophagy* **10**: 913–925.

Kanne JV, Ishikawa M, Bressendorff S, Ansbøl J, Hasebe M, Rodriguez E, Petersen M. 2022. Overexpression of ATG8/LC3 enhances wound-induced somatic reprogramming in *Physcomitrium patens*. *Autophagy* **18**: 1463–1466.

Kellner R, De la Concepcion JC, Maqbool A, Kamoun S, Dagdas YF. 2017. ATG8 expansion: a driver of selective autophagy diversification? *Trends in Plant Science* **22**: 204–214.

Kim JH, Lee HN, Huang X, Jung H, Otegui MS, Li F, Chung T. 2022. FYVE2, a phosphatidylinositol 3-phosphate effector, interacts with the COPII machinery to control autophagosome formation in Arabidopsis. *Plant Cell* **34**: 351–373.

Kriegenburg F, Ungermann C, Reggiori F. 2018. Coordination of autophagosome–lysosome fusion by Atg8 family members. *Current Biology* **28**: R512–R518.

Lan H-J, Ran J, Wang W-X, Zhang L, Wu NN, Zhao YT, Huang MJ, Ni M, Liu F, Cheng N *et al.* 2024. Clathrin light chains negatively regulate plant immunity by hijacking the autophagy pathway. *Plant Communications* **5**: 100937.

Li F, Chung T, Vierstra RD. 2014. AUTOPHAGY-RELATED11 plays a critical role in general autophagy- and senescence-induced mitophagy in *Arabidopsis*. *Plant Cell* **26**: 788–807.

Li H, Wei J, Liao Y, Cheng X, Yang S, Zhuang X, Zhang Z, Shen W, Gao C. 2022. MLKs kinases phosphorylate the ESCRT component FREE1 to suppress abscisic acid sensitivity of seedling establishment. *Plant, Cell & Environment* **45**: 2004–2018.

Liu F, Hu W, Li F, Marshall RS, Zarza X, Munnik T, Vierstra RD. 2020. AUTOPHAGY-RELATED14 and its associated phosphatidylinositol 3-kinase complex promote autophagy in *Arabidopsis*. *Plant Cell* **32**: 3939–3960.

Marshall RS, Hua Z, Mali S, McLoughlin F, Vierstra RD. 2019. ATG8-binding UIM proteins define a new class of autophagy adaptors and receptors. *Cell* **177**: 766–781.

Marshall RS, Vierstra RD. 2018. Autophagy: the master of bulk and selective recycling. *Annual Review of Plant Biology* **29**: 173–208.

McEwan DG, Popovic D, Gubas A, McEwan DG, Terawaki S, Suzuki H, Stadel D, Coxon F P, de Miranda Stegmann D, Bhogaraju S *et al.* 2015. PLEKHM1 regulates autophagosome-lysosome fusion through HOPS complex and LC3/GABARAP proteins. *Molecular Cell* **57**: 39–54.

McLoughlin F, Augustine RC, Marshall RS, Li F, Kirkpatrick LD, Otegui MS, Vierstra RD. 2018. Maize multi-omics reveal roles for autophagic recycling in proteome remodelling and lipid turnover. *Nature Plants* **4**: 1056–1070.

McLoughlin F, Marshall RS, Ding X, Chatt EC, Kirkpatrick LD, Augustine RC, Li F, Otegui MS, Vierstra RD. 2020. Autophagy plays prominent roles in amino acid, nucleotide, and carbohydrate metabolism during fixed-carbon starvation in maize. *Plant Cell* **32**: 2699–2724.

Muhammad D, Clark NM, Tharp NE, Chatt EC, Vierstra RD, Bartel B. 2024. Global impacts of peroxisome and pexophagy dysfunction revealed through multi-omics analyses of *lon2* and *atg2* mutants. *The Plant Journal* **120**: 2563–2583.

Nakatogawa H. 2020. Mechanisms governing autophagosome biogenesis. *Nature Reviews Molecular Cell Biology* **21**: 439–458.

Nieto-Torres JL, Leidal AM, Debnath J, Hansen M. 2021. Beyond autophagy: the expanding roles of ATG8 proteins. *Trends in Biochemical Sciences* **46**: 673–686.

Phillips AR, Suttangkakul A, Vierstra RD. 2008. The ATG12-conjugating enzyme ATG10 is essential for autophagic vesicle formation in *Arabidopsis thaliana*. *Genetics* **178**: 1339–1353.

Qi H, Xia F-N, Xiao S. 2021. Autophagy in plants: physiological roles and post-translational regulation. *Journal of Integrative Plant Biology* **63**: 161–179.

Rodriguez-Furlan C, Domozych D, Qian W, Enquist PA, Li X, Zhang C, Schenk R, Winbigler HS, Jackson W, Raikhel NV *et al.* 2019. Interaction between VPS35 and RABG3f is necessary as a checkpoint to control fusion of late compartments with the vacuole. *Proceedings of the National Academy of Sciences, USA* **116**: 21291–21301.

Sanmartin M, Ordóñez A, Sohn E, Sohn EJ, Robert S, Sánchez-Serrano JJ, Surpin MA, Raikhel NV, Rojo E. 2007. Divergent functions of VTI12 and VTI11 in trafficking to storage and lytic vacuoles in *Arabidopsis*. *Proceedings of the National Academy of Sciences, USA* **104**: 3645–3650.

Shin KD, Lee HN, Chung T. 2014. A revised assay for monitoring autophagic flux in *Arabidopsis thaliana* reveals involvement of AUTOPHAGY-RELATED 9 in autophagy. *Molecules and Cells* **37**: 399–405.

Singh MK, Krüger F, Beckmann H, Brumm S, Vermeer JEM, Munnik T, Mayer U, Stierhof YD, Grefen C, Schumacher K *et al.* 2014. Protein delivery to vacuole requires SAND protein-dependent Rab GTPase conversion for MVB-vacuole fusion. *Current Biology* **24**: 1383–1389.

Sláviková S, Shy G, Yao Y, Glozman R, Levanony H, Pietrokovski S, Elazar Z, Galili G. 2005. The autophagy-associated Atg8 gene family operates both under favourable growth conditions and under starvation stresses in Arabidopsis plants. *Journal of Experimental Botany* **56**: 2839–2849.

Smalle J, Kurepa J, Yang P, Babiychuk E, Kushnir S, Durski A, Vierstra RD. 2002. Cytokinin growth responses in *Arabidopsis* involve the 26s proteasome subunit RPN12. *Plant Cell* **14**: 17–32.

Sun J, Shao Y, Wang S, Li X, Feng S, Wang W, Leroy P, Li C, Zheng H. 2023. An *Arabidopsis* Rab18 GTPase promotes autophagy by tethering ATG18a to the ER in response to nutrient starvation. *Developmental Cell* **58**: 2947–2958.

© 2025 The Author(s).
New Phytologist © 2025 New Phytologist Foundation.

14698137, 0, Downloaded from https://nph.onlinelibrary.wiley.com/doi/10.1111/nph.70418 by University Of British Columbia, Wiley Online Library on [01/09/2025]. See the Terms and Conditions (https://onlinelibrary.wiley.com/terms-and-conditions) on Wiley Online Library for rules of use; OA articles are governed by the applicable Creative Commons License

Sun S, Feng L, Chung KP, Lee KM, Cheung HHY, Luo M, Ren K, Law KC, Jiang L, Wong KB *et al.* 2022. Mechanistic insights into an atypical interaction between ATG8 and SH3P2 in *Arabidopsis thaliana*. *Autophagy* **18**: 1350–1366.

Suttangkakul A, Li F, Chung T, Vierstra RD. 2011. The ATG1/ATG13 protein kinase complex is both a regulator and a target of autophagic recycling in *Arabidopsis*. *Plant Cell* **23**: 3761–3779.

Svenning S, Lamark T, Krause K, Johansen T. 2011. Plant NBR1 is a selective autophagy substrate and a functional hybrid of the mammalian autophagic adapters NBR1 and p62/SQSTM1. *Autophagy* 7: 993–1010.

Thompson AR, Doelling JH, Suttangkakul A, Vierstra RD. 2005. Autophagic nutrient recycling in *Arabidopsis* directed by the ATG8 and ATG12 conjugation pathways. *Plant Physiology* **138**: 2097–2110.

Wang P, Sun X, Jia X, Wang N, Gong X, Ma F. 2016. Characterization of an autophagy-related gene *MdATG8i* from apple. *Frontiers in Plant Science* **7**: 720.

Wang Y, Li J, Wang J, Han P, Miao S, Zheng X, Han M, Shen X, Li H, Wu M *et al.* 2022. Plant UVRAG interacts with ATG14 to regulate autophagosome maturation and geminivirus infection. *New Phytologist* **236**: 1358–1374.

Wang Z-P, Xing H-L, Dong L, Zhang HY, Han CY, Wang XC, Chen QJ. 2015. Egg cell-specific promoter-controlled CRISPR/Cas9 efficiently generates homozygous mutants for multiple target genes in *Arabidopsis* in a single generation. *Genome Biology* **16**: 144.

Weidberg H, Shvets E, Shpilka T, Shimron F, Shinder V, Elazar Z. 2010. LC3 and GATE-16/GABARAP subfamilies are both essential yet act differently in autophagosome biogenesis. *EMBO Journal* **29**: 1792–1802.

Xia K, Liu T, Ouyang J, Wang R, Fan T, Zhang M. 2011. Genome-wide identification, classification, and expression analysis of autophagy-associated gene homologues in rice (*Oryza sativa l.*). *DNA Research* **18**: 363–377.

Xia T, Xiao D, Liu D, Chai W, Gong Q, Wang NN. 2012. Heterologous expression of *ATG8c* from soybean confers tolerance to nitrogen deficiency and increases yield in *Arabidopsis*. *PLoS ONE* 7: e37217.

Xiao Z, Yang C, Liu C, Yang L, Yang S, Zhou J, Li F, Jiang L, Xiao S, Gao C *et al.* 2020. SINAT E3 ligases regulate the stability of the ESCRT component FREE1 in response to iron deficiency in plants. *Journal of Integrative Plant Biology* **62**: 1399–1417.

Xie Z, Nair U, Klionsky DJ. 2008. Atg8 controls phagophore expansion during autophagosome formation. *Molecular Biology of the Cell* **19**: 3290–3298.

Xing H-L, Dong L, Wang Z-P, Zhang HY, Han CY, Liu B, Wang XC, Chen QJ. 2014. A CRISPR/Cas9 toolkit for multiplex genome editing in plants. *BMC Plant Biology* **14**: 327.

Yan H, Lu Z, Du X *et al.* 2024. Autophagy modulates *Arabidopsis* male gametophyte fertility and controls actin organization. *Nature Communications* **15**: 10071.

Yoo S-D, Cho Y-H, Sheen J. 2007. *Arabidopsis* mesophyll protoplasts: a versatile cell system for transient gene expression analysis. *Nature Protocols* **2**: 1565–1572.

Zeng Y, Chung KP, Li B, Lai CM, Lam SK, Wang X, Cui Y, Gao C, Luo M, Wong KB *et al.* 2015. Unique COPII component AtSar1a/AtSec23a pair is required for the distinct function of protein ER export in *Arabidopsis thaliana*. *Proceedings of the National Academy of Sciences, USA* **112**: 14360–14365.

Zeng Y, Li B, Huang S, Li H, Cao W, Chen Y, Liu G, Li Z, Yang C, Feng L *et al.* 2023. The plant unique ESCRT component FREE1 regulates autophagosome closure. *Nature Communications* **14**: 1768.

Zeng Y, Li B, Ji C, Feng L, Niu F, Deng C, Chen S, Lin Y, Cheung KCP, Shen J *et al.* 2021. A unique AtSar1D-AtRabD2a nexus modulates autophagosome biogenesis in *Arabidopsis thaliana*. *Proceedings of the National Academy of Sciences, USA* **118**: e2021293118.

Zess EK, Jensen C, Cruz-Mireles N, de la Concepcion JC, Sklenar J, Stephani M, Imre R, Roitinger E, Hughes R, Belhaj K *et al.* 2019. N-terminal β-strand underpins biochemical specialization of an ATG8 isoform. *PLoS Biology* **17**: e3000373.

Zhang B, Wang Y, Zhu Y, Pan T, Yan H, Wang X, Jing R, Wu H, Wang F, Zhang Y *et al.* 2024. The MON1–CCZ1 complex plays dual roles in autophagic degradation and vacuolar protein transport in rice. *Journal of Integrative Plant Biology* **67**: 35–54.

Zhao J, Bui MT, Ma J, Künzl F, Picchianti L, de la Concepcion JC, Chen Y, Petsangouraki S, Mohseni A, García-Leon M *et al.* 2022. Plant autophagosomes mature into amphisomes prior to their delivery to the central vacuole. *Journal of Cell Biology* **221**: e202203139.

Zhao Y, Codogno P, Zhang H. 2021. Machinery, regulation and pathophysiological implications of autophagosome maturation. *Nature Reviews Molecular Cell Biology* **22**: 733–750.

Zhen X, Zheng N, Yu J, Bi C, Xu F. 2021. Autophagy mediates grain yield and nitrogen stress resistance by modulating nitrogen remobilization in rice. *PLoS ONE* **16**: e0244996.

Zheng X, Ma J, Li J, Chen S, Luo J, Wu J, Zhang K, Peng CL, Zeng Y, Kang BH *et al.* 2024. ATG8ylation facilitates an ESCRT-independent vacuolar membrane invagination in plants. Research Square.

Zhou J, Ma J, Yang C, Zhu X, Li J, Zheng X, Li X, Chen S, Feng L, Wang P *et al.* 2023. A non-canonical role of ATG8 in Golgi recovery from heat stress in plants. *Nature Plants* **9**: 749–765.

Zhuang X, Wang H, Lam SK, Gao C, Wang X, Cai Y, Jiang L. 2013. A BAR-domain protein SH3P2, which binds to phosphatidylinositol 3-phosphate and ATG8, regulates autophagosome formation in *Arabidopsis*. *Plant Cell* **25**: 4596–4615.

Zou Y, Ohlsson JA, Holla S, Sabljić I, Leong JX, Ballhaus F, Krebs M, Schumacher K, Moschou PN, Stael S *et al.* 2025. ATG8 delipidation is not universally critical for autophagy in plants. *Nature Communications* **16**: 403.

Supporting Information

Additional Supporting Information may be found online in the Supporting Information section at the end of the article.

Fig. S1 Mutations in various atg8 mutants.

Fig. S2 Transient expression of different green fluorescent protein (GFP)-fused autophagy-related proteins in atg8-9m protoplasts.

Fig. S3 Transient expression of the GFP-NBR1 fusion protein in the protoplasts of various atg8 mutants.

Fig. S4 Transient expression of GFP-fused ABNORMAL SHOOT3 (ABS3) protein in atg8-9m protoplasts.

Fig. S5 Phenotypic analysis of Arabidopsis atg8 mutants.

Fig. S6 atg8 mutants produce viable pollen.

Fig. S7 Proteomic comparisons of wild-type and atg mutants during N or C starvation.

Fig. S8 Volcano plots showing the preferential accumulation of proteins in atg8-9m vs wild-type seedlings under N or C starvation.

Fig. S9 Influence of atg8 mutation on protein abundances in specific cellular compartments/complexes in N- or C-starved Arabidopsis samples.

Fig. S10 Luciferase complementation imaging assays for the detection of RABG3-ATG8 interactions.

© 2025 The Author(s).
New Phytologist © 2025 New Phytologist Foundation.

14698137, 0, Downloaded from https://nph.onlinelibrary.wiley.com/doi/10.1111/nph.70418 by University Of British Columbia, Wiley Online Library on [01/09/2025]. See the Terms and Conditions (https://onlinelibrary.wiley.com/terms-and-conditions) on Wiley Online Library for rules of use; OA articles are governed by the applicable Creative Commons License

Fig. S11 Mutations in the GTPase region of RABG3f do not affect the RABG3f-ATG8a interaction.

Fig. S12 Sequence alignment of the Arabidopsis Rab GTPase (RABG) proteins.

Fig. S13 Intracellular distribution of the autophagy marker GFP-ATG8a in the root elongation and maturation zones of gfs9-4 seedlings.

Fig. S14 The rabg3-6m mutant exhibited an early leaf senescence phenotype under short-day conditions.

Fig. S15 RABG3 is required for the vacuolar deposition of Aleu-GFP but not for ABS3-GFP.

Fig. S16 Genetic complementation of Arabidopsis rabg3-6m with wild-type or aim-mutated RABG3f.

Notes S1 Sequences of the CRISPR/Cas9 binary vectors targeting Arabidopsis ATG8 genes.

Table S1 Oligonucleotide primers used in the study.

Table S2 Normalization protein list and values used for sample correction.

Table S3 Proteome analysis.

Table S4 Proteome raw data.

Please note: Wiley is not responsible for the content or functionality of any Supporting Information supplied by the authors. Any queries (other than missing material) should be directed to the *New Phytologist* Central Office.

Disclaimer: The New Phytologist Foundation remains neutral with regard to jurisdictional claims in maps and in any institutional affiliations.

© 2025 The Author(s).
New Phytologist © 2025 New Phytologist Foundation.

14698137, 0, Downloaded from https://nph.onlinelibrary.wiley.com/doi/10.1111/nph.70418 by University Of British Columbia, Wiley Online Library on [01/09/2025]. See the Terms and Conditions (https://onlinelibrary.wiley.com/terms-and-conditions) on Wiley Online Library for rules of use; OA articles are governed by the applicable Creative Commons License